RESEARCH ARTICLE

Special Section:
Oceanography of the 2015/16 El Niño and Global Impacts on Tropical Marine Ecosystems

Key Points:
- During 2016, the southeast tropical Indian Ocean experienced the longest and most intense marine heatwave on record from 1982
- Around tropical Australia, coastal warming was caused by shortwave radiation and latent heat flux anomalies in January and February 2016
- The 2015–2016 air-sea heat flux anomalies, weakened monsoon winds and mixed layer depth anomalies were consistent with past El Niños

Supporting Information:
- Supporting Information S1

Correspondence to:
J. A. Benthuysen,
j.benthuysen@aims.gov.au

Extreme Marine Warming Across Tropical Australia During Austral Summer 2015–2016

Jessica A. Benthuysen[1] (iD), Eric C. J. Oliver[2,3,4] (iD), Ming Feng[5,6] (iD), and Andrew G. Marshall[7] (iD)

[1]Australian Institute of Marine Science, Townsville, QLD, Australia, [2]Institute for Marine and Antarctic Studies, University of Tasmania, Hobart, TAS, Australia, [3]Australian Research Council Centre of Excellence for Climate System Science, University of Tasmania, Hobart, TAS, Australia, [4]Now at Department of Oceanography, Dalhousie University, Halifax, NS, Canada, [5]CSIRO Oceans and Atmosphere, Indian Ocean Marine Research Centre, Crawley, WA, Australia, [6]Centre for Southern Hemisphere Oceans Research, Hobart, TAS, Australia, [7]Australian Bureau of Meteorology, Hobart, TAS, Australia

Abstract During austral summer 2015–2016, prolonged extreme ocean warming events, known as marine heatwaves (MHWs), occurred in the waters around tropical Australia. MHWs arose first in the southeast tropical Indian Ocean in November 2015, emerging progressively east until March 2016, when all waters from the North West Shelf to the Coral Sea were affected. The MHW maximum intensity tended to occur in March, coinciding with the timing of the maximum sea surface temperature (SST). Large areas were in a MHW state for 3–4 months continuously with maximum intensities over 2°C. In 2016, the Indonesian-Australian Basin and areas including the Timor Sea and Kimberley shelf experienced the longest and most intense MHW from remotely sensed SST dating back to 1982. In situ temperature data from temperature loggers at coastal sites revealed a consistent picture, with MHWs appearing from west to east and peaking in March 2016. Temperature data from moorings, an Argo float, and Slocum gliders showed the extent of warming with depth. The events occurred during a strong El Niño and weakened monsoon activity, enhanced by the extended suppressed phase of the Madden-Julian Oscillation. Reduced cloud cover in January and February 2016 led to positive air-sea heat flux anomalies into the ocean, predominantly due to the shortwave radiation contribution with a smaller additional contribution from the latent heat flux anomalies. A data-assimilating ocean model showed regional changes in the upper ocean circulation and a change in summer surface mixed layer depths and barrier layer thicknesses consistent with past El Niño events.

Plain Language Summary From the southeast tropical Indian Ocean to the Coral Sea, waters across tropical Australia experienced extreme warming during austral summer 2015–2016. This widespread warming was mainly caused by changes in the atmospheric conditions related to the strong El Niño. These regions had reduced cloud cover and weakened winds, leading to enhanced oceanic heating by the atmosphere. In the Indonesian-Australian Basin and surroundings areas, the shallower mixed layer depth further intensified the near-surface warming. We used satellite sea surface temperature and a range of instruments to document the warming events near the coast and in the deeper ocean. The warmer than average conditions persisted through austral winter and weakened in spring.

1. Introduction

During austral summer 2015–2016, severe mass coral bleaching and mortality were reported in most parts of the Northern Great Barrier Reef (GBR) on a scale unlike any previously observed (GBRMPA, 2016; Hughes et al., 2017). There were reports that regions of high coral mortality were associated with the lack of coral reef fish and increased presence of sea urchins on algal covered reefs (GBRMPA, 2016). In the Gulf of Carpentaria, an extreme warming event coincided with massive mangrove die-backs (Duke et al., 2017; Harris et al., 2017) and a struggling mud crab fishery industry following poor wet seasons (NTSC, 2016). Along the North West Shelf of Australia, coral bleaching was reported at reefs and shoals between Darwin and Broome, including mortality at Scott Reef, Australia's largest oceanic reef system (AIMS, 2016). Other impacts were first noticed by fishermen and indigenous communities. For example, the Anindilyakwa Rangers reported giant clams bleaching off Groote Eylandt, and the Crocodile Island Rangers investigated reports of

the first ever recorded coral bleaching at Murrungga Island off northeast Arnhem Land (Wild, 2016). These observations demonstrate the need to understand what factors contributed to the timing and severity of the thermal stresses causing devastating impacts for tropical Australia's marine ecosystems.

These bleaching reports took place during one of the longest global-scale bleaching events in recorded history, commencing in 2014 (Heron et al., 2016). The austral summer 2015–2016 events in tropical Australia coincided with the warmest consecutive months recorded for global sea surface temperatures (NOAA, 2017). The increased likelihood of record temperatures globally in recent years has been attributed to anthropogenic climate forcing (Mann et al., 2016). Based on climate model simulations, an increased likelihood of warm Coral Sea temperatures associated with the 2016 GBR coral bleaching event was attributed to anthropogenic global warming levels (King et al., 2017).

While a widespread background warming trend may be important in raising temperatures across northern Australia (Figure 1a), in 2015–2016, the regional temperature anomalies were influenced by one of the strongest recorded El Niños since 1997–1998 (Figure 1b). The El Niño persisted through 2015 and dissipated in austral autumn 2016 (NOAA, 2017). El Niño years have been associated with a later onset and a weaker Australian summer monsoon (Allan & Pariwono, 1990; Evans & Allen, 1992; Hung & Yanai, 2004; Redondo-Rodriguez et al., 2012) related to a shift in the Walker circulation. Consistent with past El Niños, the 2015–2016 Australian summer monsoon appeared weaker than typical years, based on summer mean zonal winds (Figure 1d). El Niños are linked with reduced cloud cover and high outgoing longwave radiation across tropical Australia (Allan & Pariwono, 1990; Klein et al., 1999). As the El Niño decayed in autumn 2016 (Figure 1b), the Indian Ocean (IO) Dipole Mode index (DMI) became negative (Figure 1c), signifying warmer waters in the eastern Indian Ocean, with one of the strongest negative values during winter 2016. On the intraseasonal timescale, the Madden-Julian Oscillation (MJO; Madden & Julian, 1971, 1972) is found to influence the start of the monsoon (Hung & Yanai, 2004), the timing of monsoon bursts and breaks (Hendon & Liebmann, 1990), and may play a role in the emergence and development of marine heatwaves regionally (Zhang et al., 2017). We seek to understand these relative roles of drivers governing interannual and intraseasonal variability during the events that transpired during austral summer 2015–2016.

During El Niño, the changes in atmospheric conditions lead to regional warming patterns around Australia. In the Indonesian-Australian Basin and to the north of Australia, SST anomalies tend to rapidly transition from cool in austral spring to warm in austral summer and remain warm through to at least autumn (e.g., Zhang et al., 2017). In addition, there is a large-scale Indian Ocean basin-wide warming with a maximum in austral autumn due to the influence of El Niño on air-sea heat fluxes (e.g., Klein et al., 1999). Following the El Niño's dissipation, these warm anomalies persist through winter due to the capacitor effect, with feedback from the temperatures maintaining the anomalous atmospheric conditions (e.g., Xie et al., 2009, 2016). In the GBR, there tends to be neutral or cool SST anomalies in austral spring followed by warming through summer and peaking in early autumn (Lough, 1994, 1999; Zhang et al., 2017). The warm anomalies tend to peak 1–2 months after the climatological maximum in SST (Lough, 1999). While the warm anomalies tend to decay in autumn in the north, they persist into winter and decay in spring toward the south (Lough, 1999). For this region, the mechanisms controlling the long persistence of warm anomalies are not well understood.

The objectives of this study are to describe the spatial and temporal evolution of marine heatwaves (MHWs) across tropical Australia during 2015–2016. Our main focus is on the events occurring during the extended austral summer. This time period is the critical season for impacts in the north, as peak absolute temperatures are one of the primary factors for coral bleaching. In this study, we investigate the links between the warming patterns with potential physical drivers, including changes in the winds, air-sea heat flux, and ocean circulation. A data-assimilating ocean model is used to investigate the depth extent of the warming during the MHW development in the Indonesian-Australian Basin across to regions including the Gulf of Carpentaria, the Northern Great Barrier Reef, and the Coral Sea (see supporting information Figure S1 for a regional map). We use a MHW definition to identify events regionally and characterize the timing of the MHWs' emergence, their duration and intensity, and to compare these metrics with past events. Section 2 describes the data and methods. Section 3 details the evolution of the warming events from remotely sensed and in situ temperatures and atmospheric fluxes. Section 4 describes changes in the circulation and surface mixed layer during this period from an ocean model. Section 5 compares this event with past summers during strong El Niños. Section 6 presents the discussion and summary.
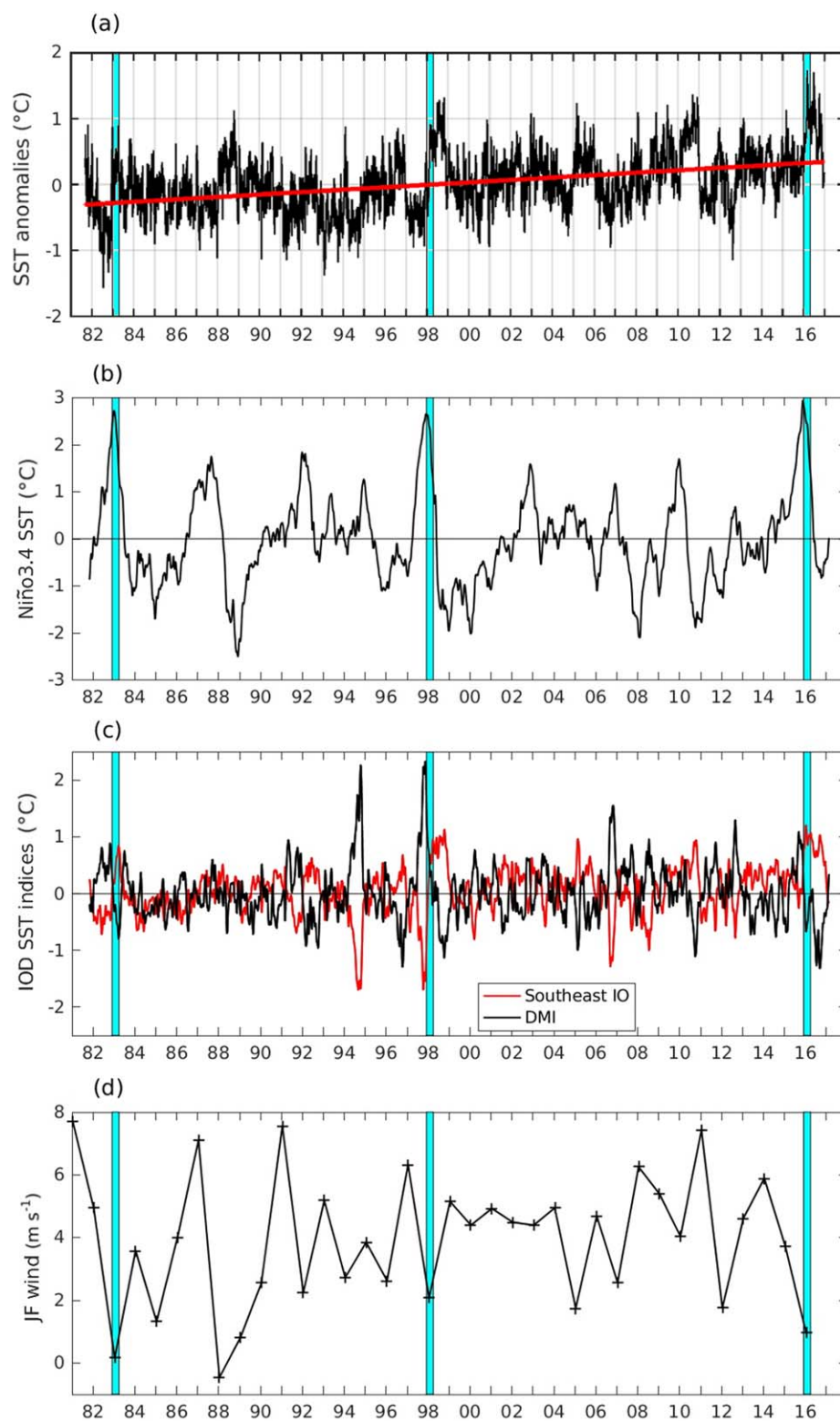
Figure 1. (a) Domain averaged (110°E–160°E, 9°S–18°S) SST anomalies based on a 1982–2015 climatology and linear trend (red line), (b) Niño3.4 index, (c) Indian Ocean Dipole (IOD) SST indices, and (d) Australian monsoon index during the 1981–2016 period. In Figure 1c, both the Dipole Mode index (DMI) and the Southeast Indian Ocean (IO) SST index are shown. A 5 point Hanning filter is applied to the weekly time series in Figures 1b and 1c. The vertical shaded bars denote the three strongest El Niños since 1981.

2. Data and Methods

2.1. Ocean Observations

Sea surface temperature (SST) is analysed using the National Oceanic and Atmospheric Administration's Optimum Interpolation Sea Surface Temperature version 2, which is a gridded analysis of the Advanced Very High Resolution Radiometer (AVHRR) satellite data (NOAA OISST V2; Reynolds et al., 2007). SST data are provided daily on a 0.25° × 0.25° horizontal resolution, and data are used from 1 September 1981 to 31 December 2016. SST data are domain averaged over five regions encompassing tropical Australia's coastal and adjacent waters (Figure 2). The regions are bounded in latitude from 9°S to 18°S and from west to east, regions are defined as the Indonesian-Australian Basin (110°E to 122°E), the Kimberley shelf and Timor Sea (122°E to 132°E), the Southern Arafura Sea and Gulf of Carpentaria (GoC) (132°E to 142°E), the Torres Strait, Northern Great Barrier Reef (GBR), and western Coral Sea (142°E to 148°E), and the Coral Sea (148°E to 160°E). An additional time series, domain averaged over all five regions, was also calculated. Anomalies for these time series were calculated by removing a climatology (see section 2.4 below for how the climatology was calculated) and linear trends were calculated by ordinary least squares regression. The Niño3.4 SST (based on 170°W–120°W, 5°S–5°N) and Indian Ocean Dipole indices, including the DMI (Saji et al., 1999), are calculated using the 1° × 1° horizontal resolution, weekly Reynolds OISST version 2 product (OI.v2; Reynolds et al., 2002), and the indices are updated weekly on the webpage: http://stateoftheocean.osmc.noaa.gov/sur/ind/setio.php.

In situ temperature measurements near the coast were available across tropical Australia since the 1990s (Figure 2; supporting information Figure S1; Table 1). Australian Baseline Sea Level Monitoring Project (ABSLMP) temperature loggers were installed on land-based structures at Cocos (Keeling) Islands, Darwin, Milner Bay (Groote Eylandt), Cape Ferguson, and Rosslyn Bay. Additional in situ temperature data were sourced from the Integrated Marine Observing System (IMOS) moorings on the northern Australian shelf at the Margaret Harries Banks site (~150 m depth) and in the Central GBR at the Palm Passage site (outer-shelf, ~70 m depth), and from the Australian Institute of Marine Science (AIMS) Data Catalogue (http://data.aims.gov.au/) near Lizard Island and Thursday Island (AIMS 2017a, 2017b, 2017c, 2017d; IMOS 2017a, IMOS 2017b). Near these islands, data from floats and reef sites were combined into homogenized time series referenced to approximately 2 m depth (see supporting information Figures S2–S5 and Tables S1 and S2).

A series of Slocum glider deployments were conducted in the Central and Northern GBR, for the first time, from October 2015 to August 2016 (Figure 2). The Slocum gliders sampled temperature and other water
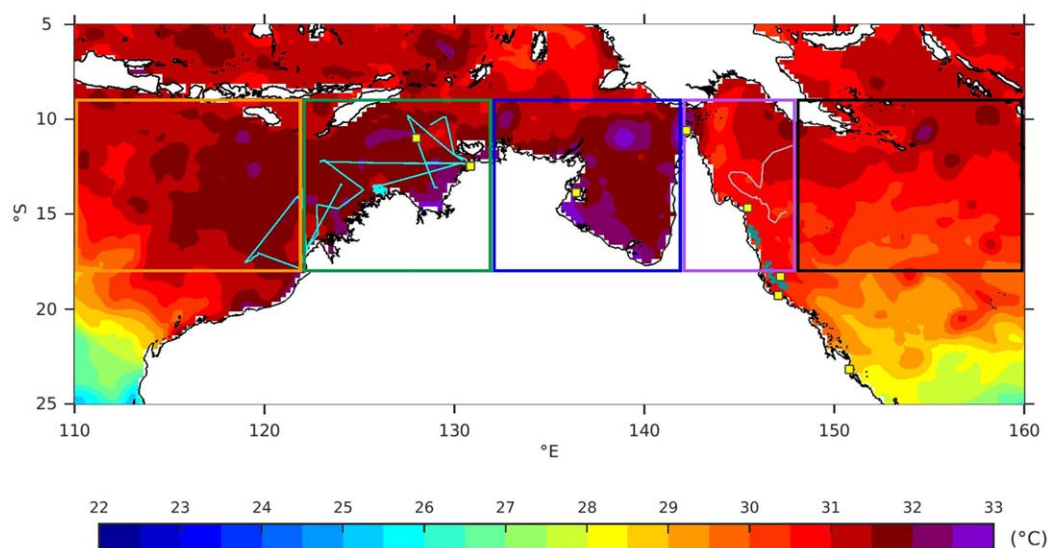

Figure 2. Map of maximum SST (NOAA OISST V2) between 1 November 2015 to 30 April 2016 and locations of in situ data. The boxed regions are defined for the Indonesian-Australian basin (orange), Kimberley shelf and Timor Sea (green), southern Arafura Sea and Gulf of Carpentaria (blue), Torres Strait, Northern Great Barrier Reef and western Coral Sea (purple), and Coral Sea (black). The in situ data are from temperature loggers (yellow squares), the R/V Solander's underway system (light blue lines), Slocum gliders in the GBR (thick turquoise lines), and an Argo float in the Coral Sea (grey line).

Table 1
In Situ Temperature Logger Sites

Site	Start date (day/month/year)	End date	Longitude (°E)	Latitude (°S)	Complete (%)
Cocos (Keeling) Islands[1]	5/9/1992	31/10/2016	96.8944	12.1167	99
Darwin[1]	2/1/1992	31/10/2016	130.8459	12.4718	87
Margaret Harries Banks[2] (20–24 m)	29/6/2010	30/7/2016	127.9998	11.0002	93
Margaret Harries Banks[2] (32–38 m)	30/5/2011	10/2/2017	127.9998	11.0002	91
Milner Bay, Groote Eylandt[1]	23/9/1993	31/10/2016	136.4156	13.8601	96
Thursday Island[3] (2.0 m)	12/5/1998	7/1/2017	142.2274	10.5835	82
Lizard Island[2,3] (2.1 m)	27/10/1995	15/12/2016	145.4460	14.6793	85
Palm Passage[2] (15 m)	7/6/2009	22/11/2016	147.1645	18.3097	94
Palm Passage[2] (60 m)	7/6/2009	22/11/2016	147.1645	18.3097	94
Cape Ferguson[1]	13/9/1991	31/10/2016	147.0584	19.2773	96
Rosslyn Bay[1]	19/6/1992	31/10/2016	150.7902	23.1610	99

Note. "Complete (%)" indicates the proportion of valid daily data in each time series as a percentage. The location and depth of the Thursday Island and Lizard Island data are for the reference data used to develop the reconstructed time series (see Supporting information). Data sources were from the Australian Baseline Sea Level Monitoring Project (ABSLMP)[1], Integrated Marine Observing System (IMOS)[2], and Australian Institute of Marine Science (AIMS)[3].

properties throughout the water column over the continental shelf, resolving the temperature structure below the surface. The processed data were obtained from the Australian Ocean Data Network (AODN) Portal (https://portal.aodn.org.au/). We used the temperature data from two deployments right after the peak of the summer marine heatwave. The deployments happened concurrently, with the first occurring from 22 March (near Cooktown) to 12 April (near Cairns), and the second occurring from 24 March (near Mission Beach) to 13 April (near Townsville). The downcast and upcast temperature data were averaged onto a vertical profile gridded at 1 m intervals.

The R/V Solander is an AIMS research vessel that traverses waters primarily along Australia's northwestern shelf. The shipboard underway thermosalinograph system has measured near-surface (1.9 m) temperature since 2010, providing near-real time in situ temperature records visualized through the AIMS Voyage Tracker (http://data.aims.gov.au/voyagetracker/). Data were obtained from the AODN Portal and AIMS Data Catalogue. We used temperature data from voyages during 6 January to 31 March 2016 (Figure 2) and compared hourly averaged data with temperature data from NOAA OISST V2.

Offshore of the GBR, an Argo float (6900905) passed through the deeper waters of the Coral Sea prior to and during the marine heatwave (Figure 2). This float was the closest one to the GBR in the Coral Sea. The processed data were obtained from the AODN Portal and Argo GDAC Data Browser, and delayed mode data were available prior to 2016. We used Argo float temperature data from August 2015 to May 2016. The temperature profiles were compared with climatological profiles from the CSIRO Atlas of Regional Seas (CARS 2009) (Ridgway et al., 2002). The climatological profiles were determined at each corresponding Argo float locations using linear interpolation of the gridded CARS 2009 data onto the location for that day.

2.2. Atmospheric Data

The Australian monsoon index is defined as the January–February average zonal wind speed at 850 mb over 110°E–130°E, 5°S–15°S based on Kajikawa et al. (2010) and is calculated from the NCEP-DOE Reanalysis 2 wind product (Kanamitsu et al., 2002). The Australian monsoon index provides a good indication of monsoonal rain across northern Australia and has been shown to be weak during El Niño years (Kajikawa et al., 2010). We used wind data and air-sea heat fluxes based on ERA-Interim (Dee et al., 2011), as used in the ocean model described below.

2.3. Ocean Model

We used data from the high resolution Bluelink reanalysis (BRAN) version 2016 (BRAN-2016) (Oke et al., 2013). BRAN derives from an integration of the Ocean Forecasting Australia Model (OFAM) and assimilates available in situ and satellite altimetry observations using the Bluelink Ocean Data Assimilation System (BODAS; Oke et al., 2013). The goal of BRAN is to provide an eddy-resolving quantitative description of the three-dimensional time-varying ocean circulation for temperature, salinity, sea level, and velocity

components for the last few decades for the seas surrounding Australia. BRAN-2016 has outward longwave, sensible, latent, and evaporative fluxes based on the current ocean state and 2 m temperature, humidity, and 10 m winds based on ERA-Interim from the European Centre for Medium-Range Weather Forecasts (Dee et al., 2011). Daily data are available from January 1994 to August 2016. The grid has 0.1° horizontal resolution, and there are 51 vertical levels in 5 km depth with 24 vertical levels in the upper 200 m. In this study we utilized the temperature, salinity, ocean velocity, and forcing (wind and air-sea heat flux) fields for the region encompassing tropical Australia. We used a mixed layer depth (MLD) definition based on 0.125 kg m^{-3} and an isothermal layer depth definition based on 0.8°C from the surface fields following Zhang et al. (2016), who applied these criteria to an earlier version of BRAN (3p5). The barrier layer thickness (BLT) is defined as the difference between the isothermal layer depth and the shallower MLD.

2.4. Marine Heatwave Definition and Metrics

To characterize the extreme marine warming of 2015–2016, we used the definition of a marine heatwave (MHW) to be an anomalously warm, discrete, and prolonged event (Hobday et al., 2016). Quantitatively, MHWs were identified as periods of time for which daily temperatures were above a defined threshold for at least five consecutive days. The threshold was taken to be the seasonally varying 90th percentile climatology, following the recommendation of Hobday et al. (2016). The climatological threshold and the mean were calculated for each calendar day from all data within an 11 day window centered on that day across all years. A percentile threshold was used, rather than an absolute value, to take into account regional and seasonal variations of what was considered "extreme." Therefore, MHW events were defined in a locally relevant context. This definition has been implemented in Python (available from https://github.com/ecjoliver/ marineHeatWaves) which was the software used here. Once a MHW was identified, we calculated a set of metrics including its start and end dates, duration (in days), maximum temperature (in °C), the maximum intensity (anomaly relative to climatological mean; in °C), and the cumulative intensity over the time period (the integral of intensity over the event duration; in °C days). These MHW metrics have been described in Hobday et al. (2016). Primary metrics include the duration, a measure of the consecutive number of days that temperature exceeds the threshold, and the maximum intensity, a measure of the greatest positive temperature anomaly during the event. The cumulative intensity is a secondary metric, representing the accumulation of heat stress, and related to similar metrics (i.e., degree heating days/weeks) used to understand ecological impacts of heat stress (Eakin et al., 2009; Liu et al., 2006). These metrics allowed us to compare the MHWs arising in 2015–2016 relative to past years. We applied the algorithm to NOAA OISST V2, at every pixel and for regional domain averaged SST as described in section 2.1, and in situ temperature data. The base period used to define the climatology was 1982–2015 for NOAA OISST V2 and the full-time period available for each individual in situ logger site.

3. Evolution of the Marine Heatwaves

3.1. SST, SST Anomalies, and MHW Metrics

From austral winter 2015, SST anomalies (SSTA) generally were weak to moderately warm everywhere across tropical Australia despite localized cooler areas (Figures 3a–3c). From northern Australia to the GBR, water temperatures were relatively cool in October 2015 (Figure 3e). Warm anomalies tended to intensify from November 2015 through March 2016, with a peak in March (Figures 3f–3j). Across tropical Australian waters, warm anomalies persisted through austral winter 2016 (Figures 3m–3o). This transition pattern is consistent with a statistically significant pattern of cool anomalies in winter-spring prior to warm anomalies in summer-autumn for El Niño periods across the Great Barrier Reef (Lough, 1999, 2007) and the Indonesian-Australian Basin (IAB; Zhang et al., 2017).

Marine heatwaves were detected across tropical Australia during the extended austral summer, $T_{ext-summer}$ (1 November 2015 to 30 April 2016, Figure 4). MHWs were first detected in the IAB in November 2015, progressing eastward, and arose in the Coral Sea between January and March 2016 (Figure 4a). The greatest maximum intensities tended to occur in March across the whole domain (Figure 4d), regardless of the start date, and the MHWs ended between April–June 2016 (Figure 4b). The month of the most intense (greatest maximum intensity) MHW aligned with the month of the maximum SST in most areas (Figures 4c and 4d). Therefore, the MHWs peaked during the most sensitive period, with respect to ecosystem tolerance limits. The duration of MHW conditions at this time were prolonged, particularly in the IAB (up to 6 months), and
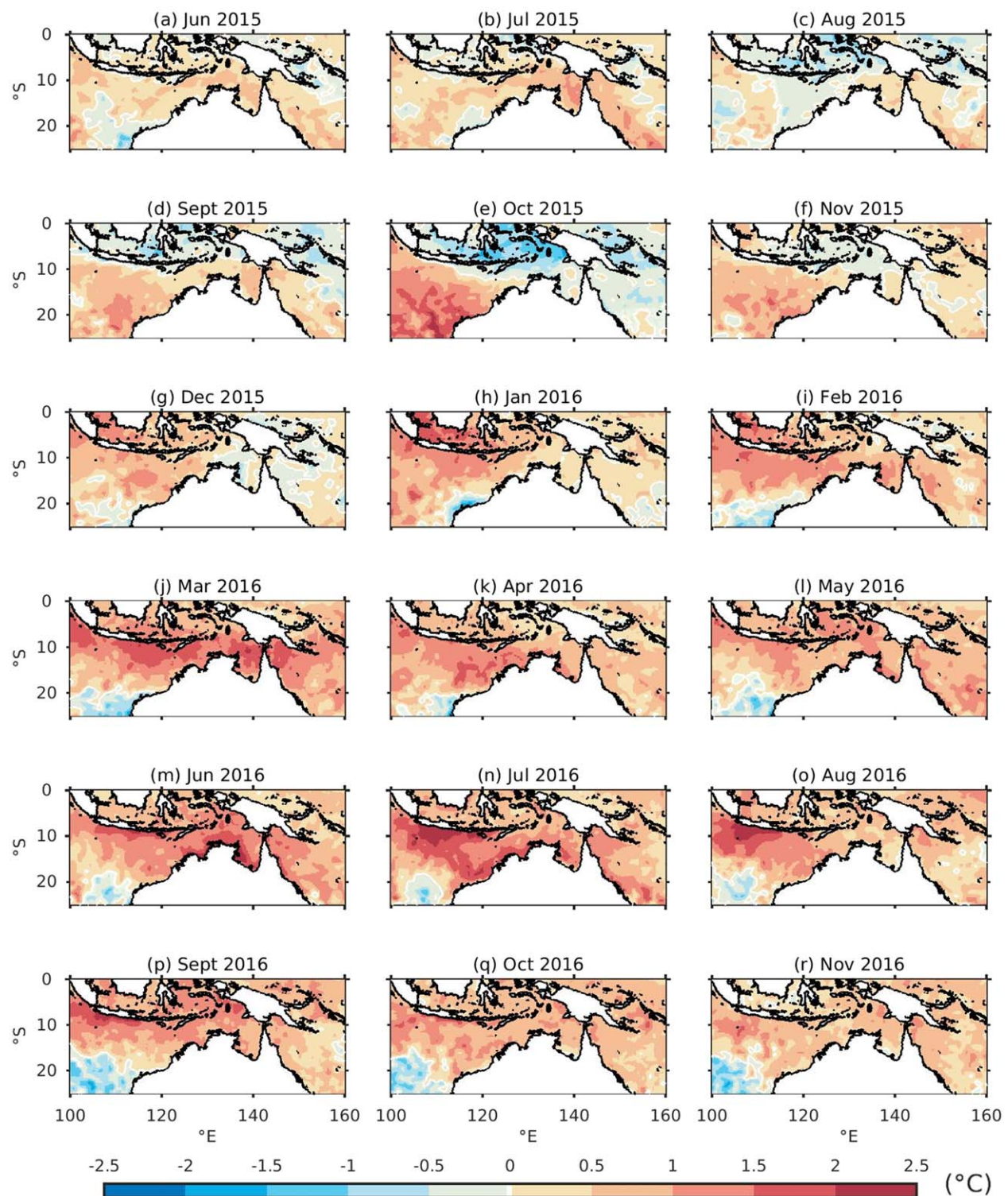
Figure 3. Monthly mean SST anomaly (SSTA) from NOAA OISST V2.

in coastal areas in the GoC and in the Northern GBR (3–4 months; Figure 4e). These areas of prolonged duration were associated with the most intense MHWs, with the greatest MHW maximum intensity exceeding 2°C across most of tropical Australia (Figure 5f).
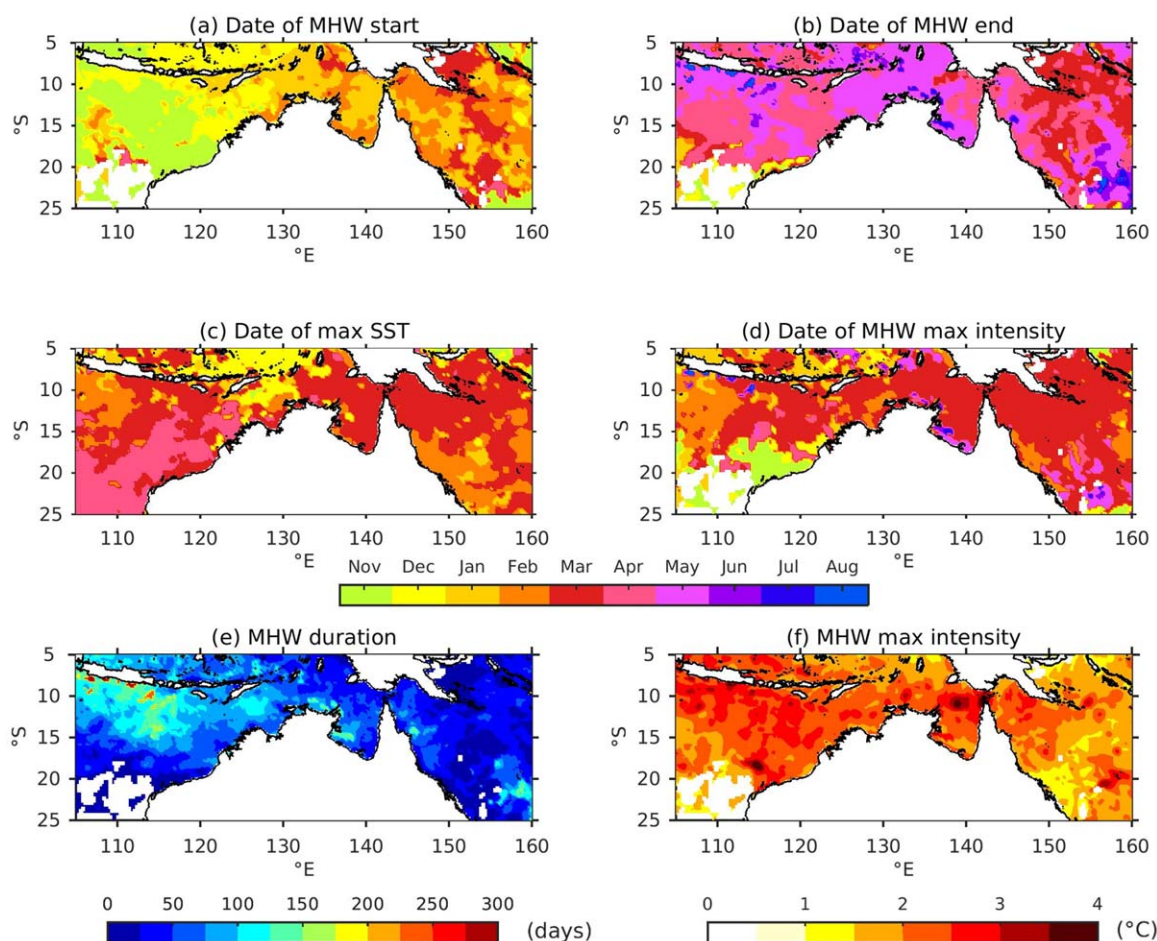
Figure 4. MHW metrics derived from NOAA OISST V2: (a) Start date of the first MHW detected in the extended-austral summer period, $T_{ext-summer}$ (1 November 2015 to 30 April 2016); (b) End month of the last MHW detected which commenced during $T_{ext-summer}$; (c) Date of maximum SST corresponding to Figure 2; (d) Date of MHW maximum intensity corresponding to plot f; (e) the total duration of all MHWs which commenced during $T_{ext-summer}$; (f) the greatest maximum intensity from all MHWs during $T_{ext-summer}$. The white ocean areas indicate regions in which no MHWs were detected during $T_{ext-summer}$.

Over the five regions across tropical Australia (Figure 2), the domain averaged SSTs revealed the regional timing of the maximum SST and maximum MHW intensity from the past several years. For 2016, all regions had a maximum SST (Figure 5) in early March, with greater values in the shallower shelf regions rather than offshore. Notably, the maximum SSTs occurred 1–3 months after climatological SST maximums except for the IAB (Figure 5). As above, MHW events emerged first in the IAB in spring 2015 and then arose in all regions by January 2016 (Figures 4a and 5). This eastward emergence of marine heatwaves was consistent with SST anomaly patterns based on composites from El Niño years (Zhang et al., 2017). This pattern was related to the intensity and spatial patterns of the air-sea heat flux anomalies and the passage of the MJO, which is discussed in section 3.4. Most events ended by May 2016 (Figure 4b) when the 2015–2016 El Niño dissipated. However, through winter 2016, MHWs continued to develop and persist, with most events ending by spring 2016 (Figure 5).

Compared with past MHW events in the five regions, record-breaking MHWs occurred in 2016. In the IAB and Kimberley shelf-Timor Sea regions, 2016 MHW events were the longest (blue lines) and the most intense (red shading) on record (Figures 5b and 5d). For both regions, the longest MHW occurred in summer-autumn 2016 (Table 2) and this coincided with the 3rd most intense MHW (+1.86°C, on 12 March 2016) in the IAB and the 4th most intense MHW (+1.94°C, on 3 March 2016) in the Kimberley shelf-Timor Sea region.

The S. Arafura Sea-GoC region had the longest MHW on record during summer-autumn 2016, and it coincided with the 3rd most intense MHW (+2.10; 11 March 2016). This region had the second greatest
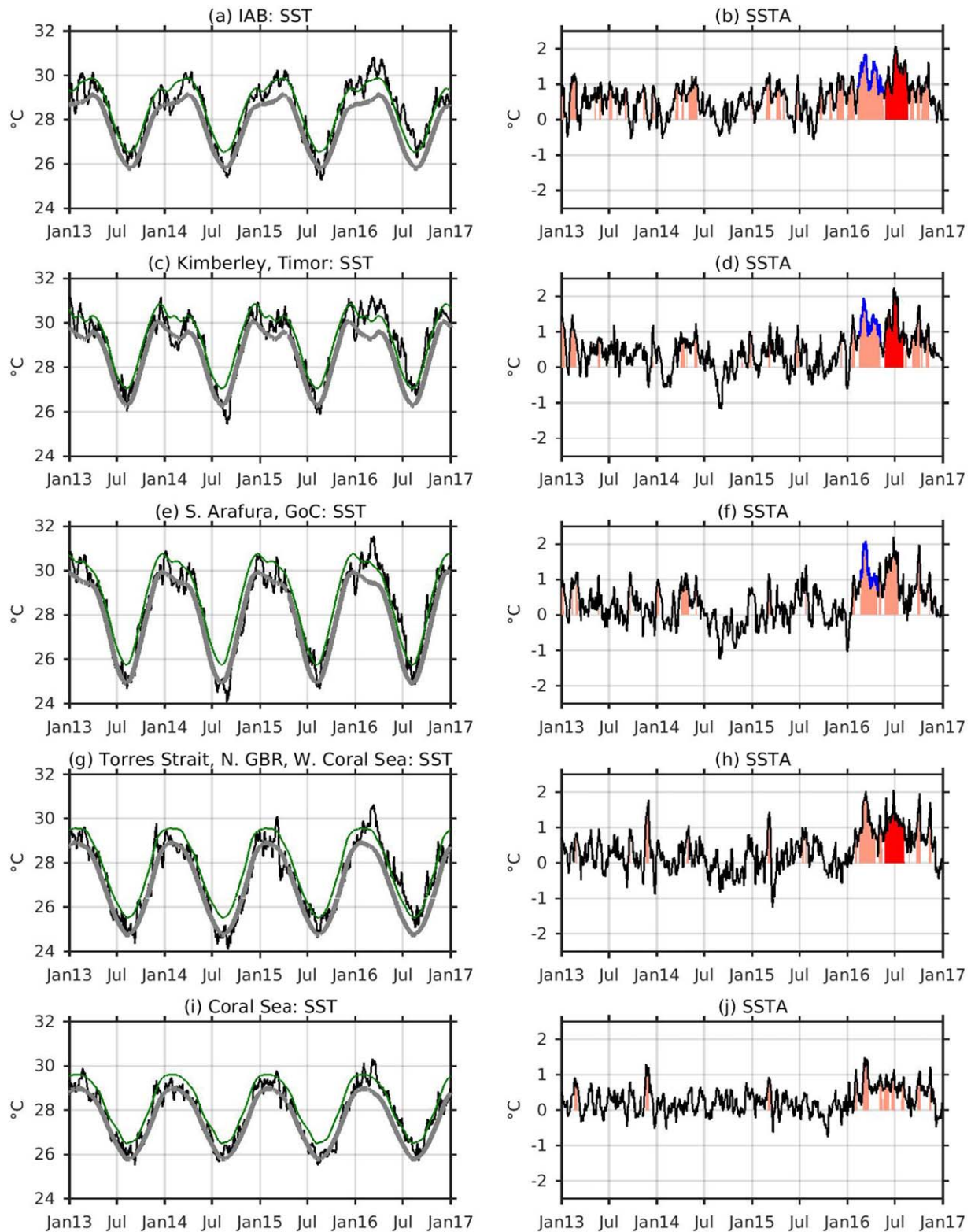
Figure 5. Domain averaged SST (left plots) and anomalies (right plots) from NOAA OISST V2. In the left plots, the curves correspond to the SST (black), the 90th percentile seasonally varying threshold (green), and the climatology (grey). Time series are presented top to bottom from west to east boxed regions. The shaded regions indicate marine heatwaves detected using the Hobday et al. (2016) definition. The pink shaded area indicates a MHW, the red shaded area includes the most intense MHW on record based on maximum intensity and the blue line indicates the longest duration MHW on record. In 2016, maximum SST (and date of occurrence) were: (a) 30.83°C (12 March 2016), (c) 31.24°C (4 March 2016), (e) 31.55°C (11 March 2016), (g) 30.64°C (11 March 2016), (i) 30.33°C (7 March 2016).

Table 2
MHW Metrics Derived From NOAA OISST V2 for the Boxed Regions

Boxed region	Number of MHW events: total (for 2016)	Maximum intensity: mean (standard deviation)	Duration: mean (standard deviation)	2016: greatest maximum intensity (Normalized) date of peak	2016: longest duration (Normalized) start/end date	2016: total duration
Indonesian-Australian basin	85 (6)	1.19°C (0.29°C)	15 days (17 days)	2.08°C (3.06) 3 Jul 2016 1.86°C (2.30) 12 Mar 2016	100 days (5) 10 Feb to 19 May 2016 91 days (5) 24 May to 22 Aug 2016	279 days
Kimberley shelf, Timor Sea	87 (7)	1.25°C (0.30°C)	13 days (12 days)	2.24°C (3.27) 27 Jun 2016 1.94°C (2.30) 3 Mar 2016	82 days (6) 15 Feb to 6 May 2016 74 days (5) 23 May to 4 Aug 2016	231 days
S. Arafura Sea, GoC	88 (6)	1.31°C (0.30°C)	13 days (10 days)	2.20°C (2.89) 26 Jun 2016 2.10°C (2.56) 11 Mar 2016	66 days (5) 20 Feb to 25 Apr 2016 54 days (4) 22 May to 14 Jul 2016	161 days
Torres Strait, N. GBR, W. Coral Sea	88 (7)	1.31°C (0.31°C)	14 days (16 days)	2.05°C (2.38) 26 Jun 2016 2.01°C (2.25) 11 Mar 2016	79 days (4) 21 May to 7 Aug 2016 64 days (3) 14 Feb to 17 Apr 2016	200 days
Coral Sea	87 (8)	1.07°C (0.21°C)	13 days (13 days)	1.49°C (2.02) 7 Mar 2016) 1.16°C (0.43) 27 June 2016	26 days (1) 28 Feb to 24 Mar 2016 24 days (1) 18 May to 10 Jun 2016	119 days

Note. The number of MHW events is shown for the full period (1 September 1981 to 31 December 2016) and for 2016 alone (parentheses). The normalized maximum intensity and duration are found by subtracting the mean and dividing by the standard deviation. For 2016, the top two events in greatest maximum intensity and duration are shown, including the normalized values.

maximum intensity on record (+2.20°C; 26 June 2016), nearly reaching the most intense one (+2.21°C; 26 February 2005). However, the March 2016 event had the greatest cumulative intensity (84°C days), followed by the June 2016 event (82°C days). In comparison, the February 2005 event had the 6th greatest cumulative intensity (30°C days) owing to a shorter duration.

The Torres Strait-N. GBR-W. Coral Sea region had the most intense MHW (+2.05°C) on 26 June 2016 (Table 2) and the second most intense MHW (+2.01°C) on 11 March 2016. In the Coral Sea region, the second most intense MHW (+1.49°C) occurred on 7 March 2016 (the 6th greatest cumulative intensity, 30°C days), while the most intense MHW (+1.95°C) occurred on 16 December 2008 (the 2nd greatest cumulative intensity, 72°C days). For these two domains, the longest duration MHW occurred in winter-spring 2010.

From 1982–2016, the maximum intensity and total duration of MHWs in each region for both annual and the extended austral summer periods revealed that 2015–2016 had extreme values compared with previous years (Figure 6). Given that the scale of the mean and variations for each metric were different per region, the metrics were normalized by the mean and standard deviation for each region across all events. In 2016, for all regions but the Coral Sea region, the greatest normalized maximum intensities were 2.38–3.27 and the longest normalized durations were 4–6 (Table 2), with both metrics far exceeding one standard deviation. For the Coral Sea region, in 2016, the greatest normalized maximum intensity was 2.02 and the longest normalized duration was 1, indicating that the scale of the event was not as extreme as in the other regions. This difference may be due to spatial variations in the air-sea heat flux anomalies, influences from the large-scale circulation, and vertical mixing with deeper cooler water in the Coral Sea. In addition, for other regions that are shallow, such as the GoC, or include continental shelves, the warming may be confined over a finite depth. These differences are further explored in the air-sea heat flux anomalies in section 3.3 and the ocean model in section 4.

3.2. In Situ Observations: Temperature Loggers, R/V Solander, Argo Float, Slocum Gliders

At shelf locations around tropical Australia, long time series of near-surface and subsurface temperatures showed warm anomalies and MHWs in 2016 (Figure 7). The timing of the MHWs largely coincided with those from the domain averaged remotely sensed SST, showing warm anomalies emerging by January 2016. Warm anomalies throughout 2016 were most evident at the Margaret Harries Bank, Darwin, Groote Eylandt, Thursday Island, Lizard Island, and Palm Passage sites. Weaker anomalies were evident further west at Cocos (Keeling) Islands and further east and south at Cape Ferguson and Rosslyn Bay. Nonetheless, every site recorded MHWs for a substantial portion of 2016 (Figure 7, shaded regions) with Darwin, Groote Eylandt, and Thursday Island recording their most intense events in 2016 (Figure 7, red shaded regions) and Darwin, Groote Eylandt, and Lizard Island recording their longest events in 2016 (Figure 7, blue lines). At Milner Bay (Groote Eylandt), the monthly mean ocean temperature of 31.9°C was a record-high for March since
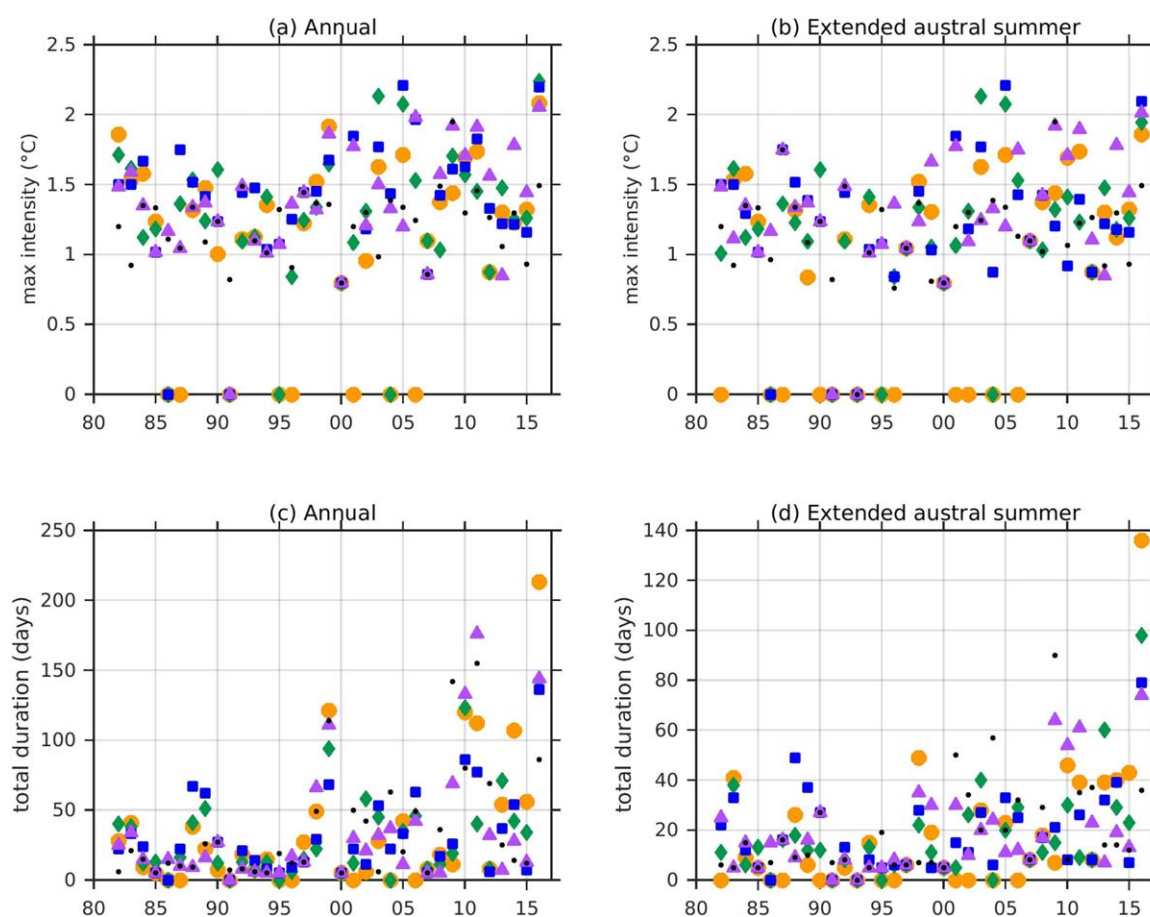
Figure 6. MHW metrics derived from NOAA OISST V2 based on each boxed region in Figure 2. The metrics correspond to the MHW with the maximum intensity (a, b) and the total duration of all MHWs (c, d) calculated annually (1 July to 30 June) or during $T_{ext-summer}$ (1 November to 30 April). The year plotted is for the end of the annual period. The years in which no MHW is detected are indicated by a zero maximum intensity. For plots a and c, MHW metrics for 1982 were only available from 1 September 1981 to 30 June 1982.

1993 (Bureau of Meteorology, 2016a). Based on these sites, we can conclude that the MHW was most intense at coastal sites across a region stretching from the Australian northwestern shelves, through the GoC and into the Torres Strait and the Northern GBR.

From January to March 2016, the R/V Solander sampled waters over the Australian North West Shelf. The first trip commenced from Broome (triangular transect) and recorded relatively cool temperatures in early January 2016 (Figure 8a). From comparison with MHW metrics derived from daily NOAA OISST V2 (Figure 8b), these waters were not in a MHW at this time. From mid to late January, the ship crossed north from Broome to Ashmore Reef (122.97°E, 12.22°S) and then east to Darwin. MHWs were first detected early on in this voyage and then waters remained in a MHW over a broad extent. SST anomalies remained typically between +1.3–2.3°C although reached +2.5°C closer to the Kimberley coast (not shown). From early to mid-February, the ship went northwest from Darwin and then southeast, and these waters were not in a MHW although SST anomalies were +0.5–1°C most of the time. From late February to mid-March, the ship went from Darwin to waters off Kalumburu (126.64°E, 14.29°S) on the Kimberley coast, and waters were in a MHW throughout the voyage. Finally, in late March, the ship traveled northeast of Broome along a single transect to Heywood (124.05°E, 13.45°S) and Echuca (123.91°E, 13.92°S) Shoals, and with relatively cooler waters, the waters were not in a MHW during this time. These patterns showed that while waters exceeded the 90th percentile for a broad spatial and temporal extent, there was regional, smaller scale variability when compared with the domain averaged temperature fields.

In the Central and southern part of the Northern GBR, two Slocum gliders were deployed nearly simultaneously in March 2016. As they traversed the continental shelf and through reef passages, the glider
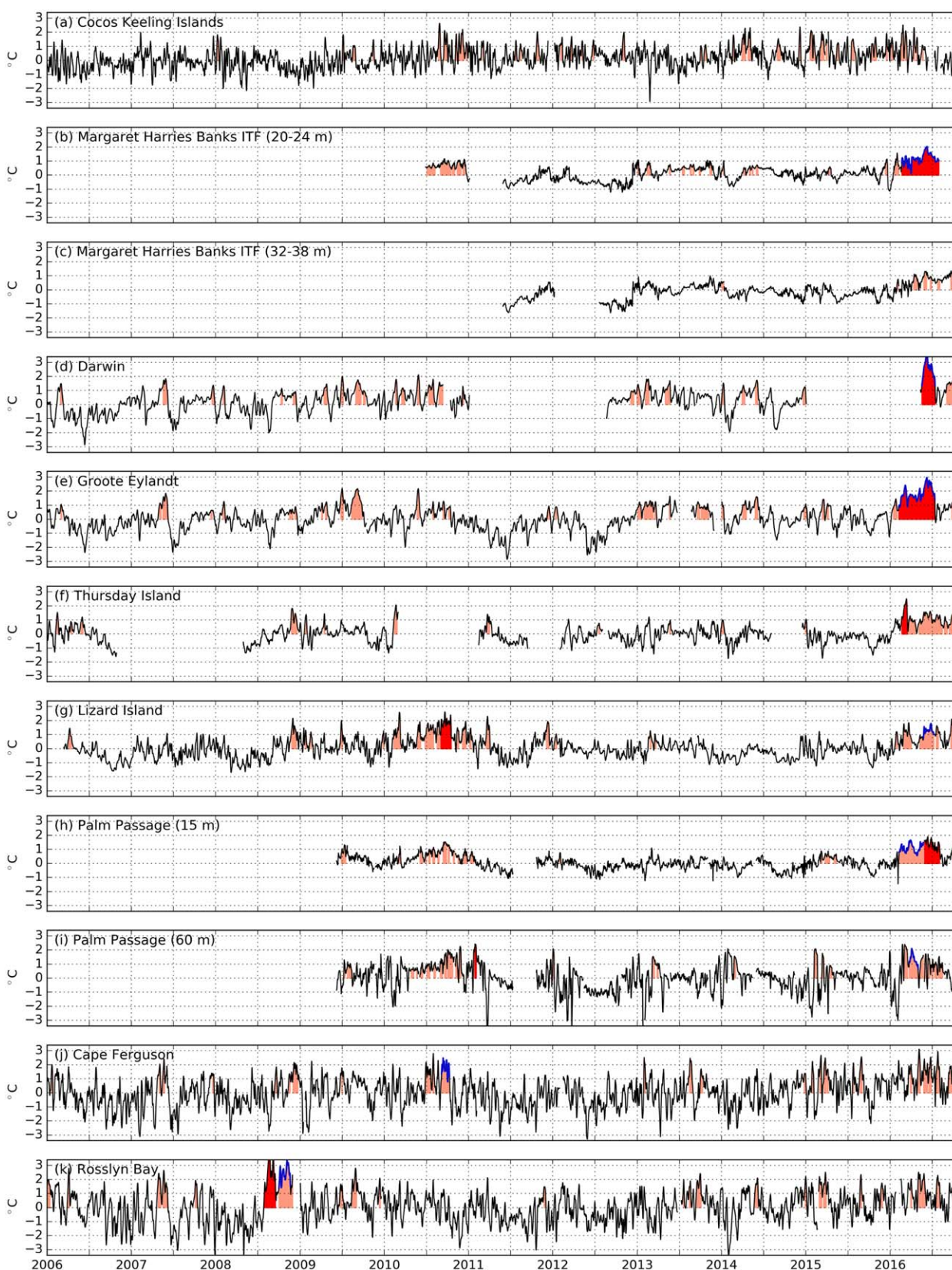
Figure 7. In situ temperature anomalies from sites across tropical Australia and the Indian Ocean. Time series are presented top to bottom from west to east. The shading is the same as described in the Figure 5 caption.
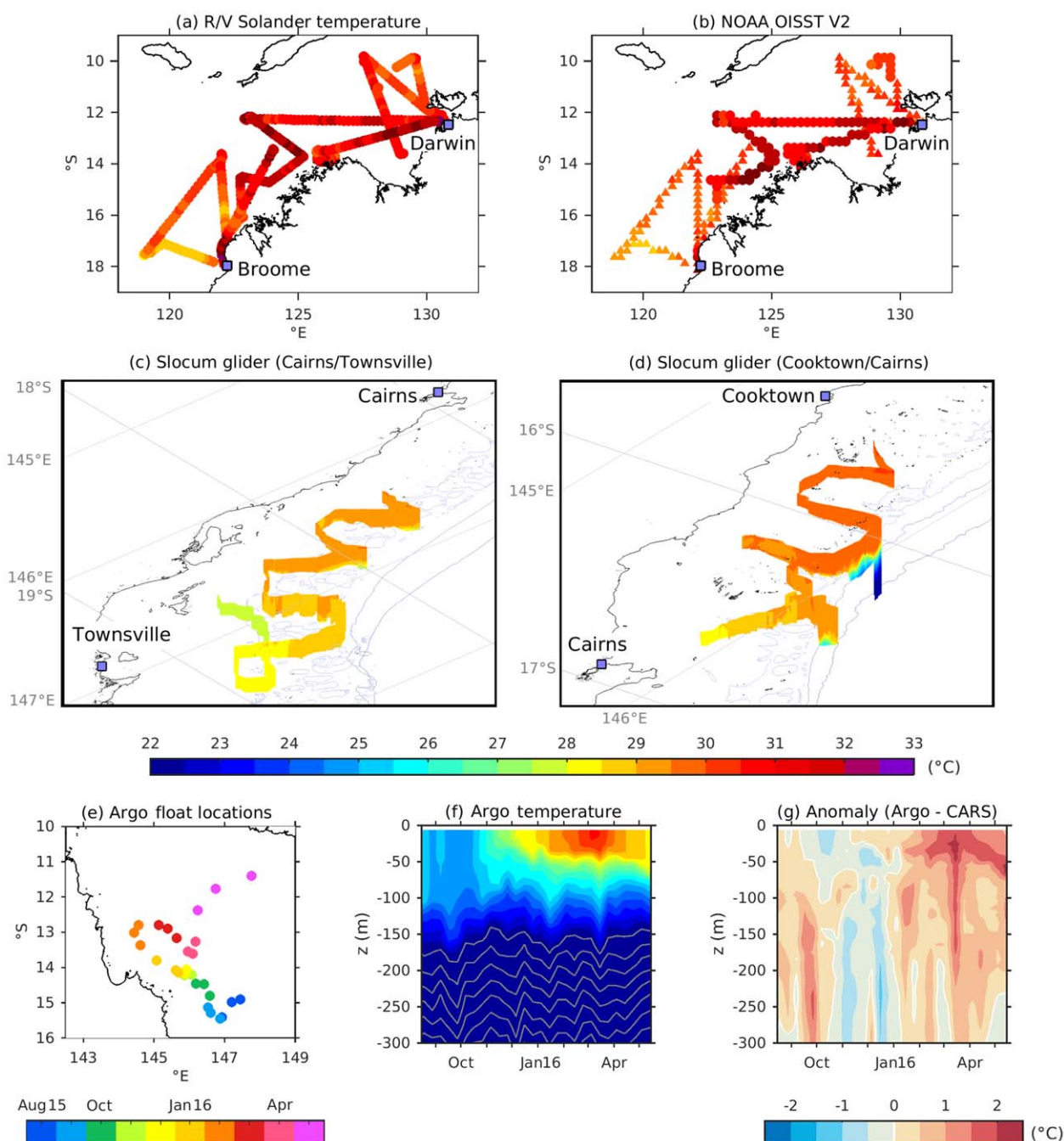
Figure 8. (a) Near-surface, hourly averaged temperatures from the R/V Solander off the North West Shelf from January to March 2016; (b) NOAA OISST V2 temperatures from the nearest ship data point with waters in a MHW (circle) and not in a MHW (triangle); (c) Slocum glider temperature from near Cairns to Townsville (24 March to 19 April 2016); (d) Slocum glider temperature from near Cooktown to Cairns (22 March–12 April 2016). In plots c and d, the coastline is in black and the 50, 100, and 200 m bathymetry contours (from gbr100) are plotted with increasing darkness of blue. (e) Location from Argo float (6900905) in the Coral Sea; (f) Argo float temperatures with grey contours every 1°C, up to 22°C; (g) Argo temperature anomaly with respect to CARS 2009.

temperatures revealed that the warm waters extended throughout the water column (Figures 8c and 8d). In the reef passages off Townsville, the typical March outer-shelf temperatures can be cooler by up to several degrees along the bottom due to intrusive upwelling or well-mixed with the transition into April with the seasonal breakdown of the stratification (Benthuysen et al., 2016). Intrusive upwelling has been associated with weakening or a reversal in the southeasterly winds during the monsoon season (Benthuysen et al., 2016). For March 2016, this region's surface waters had average SST anomalies of $+1 - 1.5$°C, and given the

weak stratification present, the temperature anomalies were likely greater near the bottom. In fact, at the nearby Palm Passage mooring site (Figures 7h and 7i), temperature anomalies were greater at depth (60 m) than near the surface (15 m) during March 2016. The vertical extent of warming over the shelf might explain why coral bleaching did not appear affected by depth and was recorded even at 25 m on some reefs (GBRMPA, 2016). The well-mixed conditions may have been associated with the passage of tropical cyclone Winston earlier that month (Figure 7 in Bainbridge, 2017), and sustained southeasterly winds may have limited intrusive upwelling and its capacity to cool the benthos.

From August 2015 to May 2016, an Argo float (6900905) in the Coral Sea passed westward toward Australia, deflected northward sampling waters off the Northern GBR, and then returned offshore (Figure 8e). As the float progressed northward, waters in the upper 100 m increased in temperature as it sampled warmer waters to the north and as spring transitioned into summer. From January to April 2016, the float was within an approximately 1° latitudinal band. The peak warming occurred in March 2016 (Figure 8f), although the maximum climatological SST within this domain occurred in late January (Figure 5g) and February in the Coral Sea (Figure 5i). The timing of the peak was consistent with the March maximum from remotely sensed temperatures in this region (Figure 5h). Compared with climatological estimates from CARS 2009, the warm anomalies tended to be most intense in the upper 50 m, up to +2.32°C in mid-March. Warm anomalies were found down to 300 m (Figure 8g), and hence the MHW event in the western Coral Sea was not confined to the near-surface but extended down into the upper ocean.

Using these in situ data, we are able to report on the 2015–2016 marine heatwaves spanning the southeast tropical Indian Ocean to the Coral Sea based on sustained monitoring of ocean temperatures over decades and technological advances in observing the ocean. This multi-instrument approach offers a complementary way of observing the MHWs to remotely sensed SSTs. The main findings here reveal that MHWs had a local maximum in intensity in March 2016 across all regions, and the vertical extent of the MHWs was substantial where observed and hence important for describing the subsurface nature of the MHWs.

3.3. Atmospheric Heat Flux and Wind Stress

The Australian monsoon is generally weakened during El Niño (e.g., Kajikawa et al., 2010; Meehl & Arblaster, 1998; Zhang et al., 2017), meaning reduced cloud cover, less rainfall, and weaker monsoon winds than normal. In the austral summer when the El Niño peaks, positive shortwave radiation anomalies and latent heat flux anomalies contribute to substantial air-sea heat flux into the ocean across the north of Australia (see supporting information Figure S7 in Zhang et al., 2017). We present here the timing and spatial patterns of the summer atmospheric conditions, set-up by the strong El Niño (Figure 1b), that contributed to the strong air-sea heat flux into the ocean across tropical Australia, followed by the autumn and winter conditions.

For early 2016, the Australian monsoon index was low (Figure 1d), which tends to occur during El Niños, signifying reduced monsoon rainfall across the north of Australia. The overall atmospheric heat flux was anomalously high during the 2016 MHWs, which would have warmed the upper ocean significantly (Figure 9). In December 2015, the heat flux anomalies were negative to the north of Australia with monthly mean values down to about -50 Wm^{-2} stretching from the Kimberley shelf in the west across to the Gulf of Carpentaria in the east (Figure 9c). However, by January 2016, these heat fluxes were anomalously high with values up to $\sim$100 Wm^{-2} (Figure 9f), coinciding with the MHWs arising across the north (Figure 4a). In February 2016 these anomalies persisted, perhaps slightly weakened over the north but intensifying over the IAB, along the GBR, and areas to the southwest of the Kimberley shelf (Figure 9i). The continued positive air-sea heat flux anomalies led to the MHWs arising in the GBR and Coral Sea (Figure 4a). By March 2016 heat fluxes had relaxed to near-normal conditions (Figure 9l). We have decomposed the contributions of shortwave radiation and latent heat flux to the total, and found that shortwave radiation was primarily responsible for the anomalous heat fluxes in January and February 2016.

From April–July 2016, positive air-sea heat flux anomalies into the ocean occurred during early winter. The extended warming and subsequent winter peak in MHWs (Figure 5) were caused primarily by positive latent heat flux anomalies (supporting information Figure S6). Off northwest Australia, the wind-evaporation-SST feedback (e.g., Nicholls, 1979; Xie & Philander, 1994) may have been operating to intensity the SST anomalies there. In this region, mean southeasterly winds (supporting information Figure S7) were opposed by
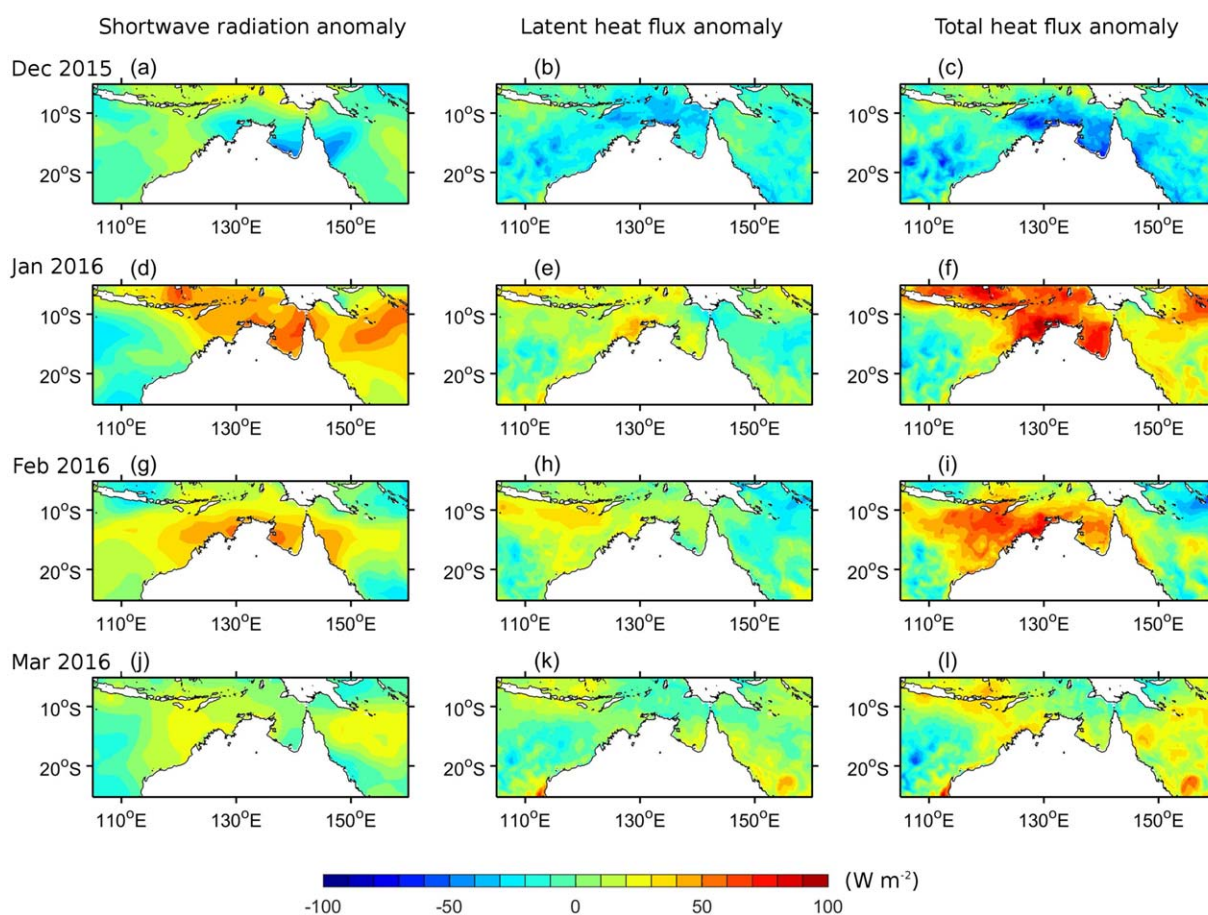
Figure 9. Air-sea heat flux anomalies derived from BRAN-2016. a, d, g, j (left plots) Anomalies from shortwave radiation, b, e, h, k (middle plots) latent heat flux, and c, f, i, l (right plots) total heat flux are presented for December 2015 (Figures 9a–9c), January 2016 (Figures 9d–9f), February 2016 (Figures 9g–9i), and March 2016 (Figures 9j–9l). Positive values are into the ocean.

westerly wind anomalies (supporting information Figure S8), leading to reduced evaporative cooling. Meanwhile, over the GBR and Coral Sea, anomalous anticyclonic winds weakened the southeasterly trade winds, reducing latent heat loss from May to July. Although the El Niño had dissipated by winter, these air-sea heat fluxes contributed to a second peak in MHWs across almost all regions (Figure 5).

3.4. MJO's Role on Summer Conditions

During austral summer 2015–2016, subseasonal variations in the evolution of the MHWs were provided by a very active MJO. An MJO event rapidly intensified with active convection over the Maritime Continent and northern Australia around mid-December, bringing heavy rainfall to the GoC, and the northwest Coral Sea with the emergence of an active monsoon trough and enhanced monsoon westerlies (Bureau of Meteorology, 2016b). The northern Australian wet season had a relatively early start considering the concurrent El Niño event which would usually delay the monsoon onset date to around late December/early January (e.g., Joseph et al., 1991). The MJO's influence on cloudiness and rainfall over northern Australia was evident with a strong reduction in outgoing longwave radiation in the second half of December (supporting information Figure S9), before the MJO convective envelope moved east of the Australian region in January 2016. As the MJO event propagated further east, its suppressed convective phase emerged over tropical Australia, bringing about a break in the Australian monsoon with above average temperatures, and below average rainfall throughout most of January (Bureau of Meteorology, 2016c). An associated increase in solar insolation is evident directly north of Australia at this time (Figure 9d). In addition, reduced westerly flow (Figures 10c and 10d) led to weakened evaporative cooling and decreased latent heat loss (Figure 9e). Meanwhile, a gradual decrease in the Niño3.4 SST (Figure 1b) indicated that the El Niño event had peaked and was beginning to subside.
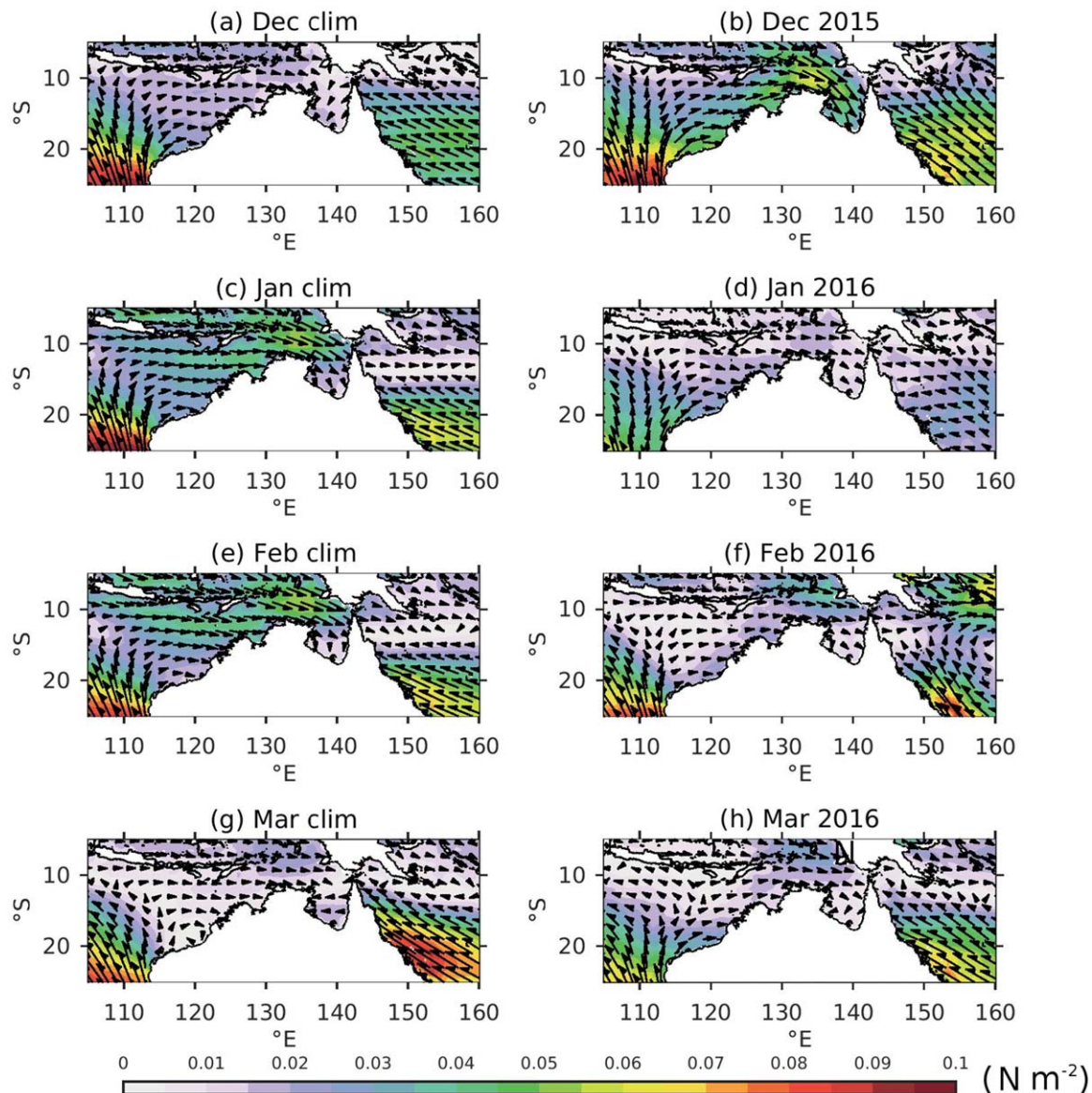
Figure 10. Wind stress from ERA-Interim, as applied in BRAN-2016, for December (a, b) to March (g, h). The monthly averaged wind stress based on a climatology period (clim) from 1994 to 2015 (left plots) is compared with monthly averages during austral summer 2015–2016 (right plots).

In late January and early February 2016, active MJO convection returned to the Maritime Continent/northern Australian region, contributing again to a burst in Australian monsoon rainfall with an associated trough over the Northern Territory and a reduction in outgoing longwave radiation (OLR) over tropical Australia (supporting information Figure S9). However this monsoonal activity was short-lived and relatively weak, despite the presence of the MJO, because the monsoon flow shifted equatorward due to a southerly wind stream from the Australian continent (Bureau of Meteorology, 2016d). This failure in monsoonal activity led to warm air temperatures, below average rainfall, and increased OLR (supporting information Figure S9) across northern Australia throughout most of February (Bureau of Meteorology, 2016d). This again constituted a subsequent increase in shortwave radiation, weakened latent heat loss, and an increase of net heat flux over the MHW region (Figures 9g–9i).

In March, the MJO completed another full cycle, traversing the Western Hemisphere and Indian Ocean in the first half of the month before again intensifying with active convection over the Maritime Continent and northern Australia from mid-March. Accordingly, a reduction in cloud cover and rainfall across tropical

Australia in early March was soon replaced with a monsoon burst/trough and tropical low off Queensland, leading to a brief respite from the unusually warm and dry conditions (Bureau of Meteorology, 2016e). Later that month and into April, as the MJO continued further east and weakened in its lifecycle, suppressed rainfall conditions returned to tropical Australia, and the monsoon season came to an end. Hence, while the strong El Niño set-up the overall atmospheric conditions instigating the MHWs, the MJO played an important role in modulating the monsoon winds and air-sea heat fluxes during the austral summer months.

4. Upper Ocean Circulation and Structure

We examined the upper ocean structure during February when reduced monsoon winds and enhanced air-sea heat flux anomalies occurred, immediately before the marine heatwaves reached a maximum intensity in early March 2016. Based on the climatology, the dominant circulation patterns consist of a westward flowing South Equatorial Current along the southern side of Java and a southwestward flow through the Timor Strait, connected from the Indonesian Throughflow (ITF), and a cyclonic circulation in the GoC. In the Coral Sea, the upper ocean currents have westward flow associated with the jets from the South Equatorial Current (Figure 11a), and near the GBR, the westward currents bifurcate into the equatorward flowing Gulf of Papua Current, and the poleward flowing East Australian Current. The East Australian Current tends to intensify to the south of the bifurcation along the slope at the edge of the GBR. We considered whether changes in the boundary currents could have contributed to the marine heatwaves through strengthening and the transport of heat.

In February 2016, the depth averaged (upper 100 m) velocities in the IAB revealed a reduced South Equatorial Current (Figure 11), consistent with a weaker ITF during El Niño (Du et al., 2008). Over the northwestern shelves and in the GoC, the upper ocean currents do not reveal notable differences in speed or direction. In the western Solomon Sea, 2016 currents were intensified and consistent with the characteristic of higher eddy kinetic energy following an El Niño event (Melet et al., 2010), and the Coral Sea had a more complex, eddy-rich field (Figure 11b). The Gulf of Papua Current appeared stronger in 2016 than in past years (Figure 11c). Meanwhile, eddy features appeared to modulate locally the strength of the East Australian Current along the shelf-edge. We do not find a clear link between the changes in the broad-scale currents examined here and the marine heatwave events. This suggests that it was primarily the air-sea heat fluxes that dominated the large-scale warming patterns rather than by horizontal advection causing a build-up of heat prior to the peak of the event. However, changes in the upper ocean density structure may have contributed to the intensity of the marine heatwaves, which were more intense in the IAB than the Coral Sea.

Compared with previous years, the February 2016 mixed layer depth (MLD) was reduced by ~5–10 m in the IAB (Figures 12a, 12c, 12e and 13a). In the Coral Sea, the MLD anomaly was less pronounced and varied in regions as deeper or shallower than normal by 0–5 m (Figure 12c). The barrier layer thickness (BLT) was reduced primarily in the northern IAB and the Gulf of Papua and Coral Sea by ~5 to 15 m (Figures 12b, 12d, and 12f). In the Coral Sea west of 160°E, the MLD can deepen by ~3–6 m based on a coupled ocean-atmosphere model, owing to enhanced evaporation over precipitation, and the MLD anomaly depends on the net buoyancy flux (Zhang et al., 2015). In the southeast tropical Indian Ocean (SETIO), the MLD, and BLT have been shown to shoal by ~4–12 m in summer months during El Niño events (Zhang et al., 2016) consistent with these results. The reduced BLT may be due to increased salinity associated with El Niño events (Zhang et al., 2016). A reduced MLD is likely associated with weakened wind speeds (Figures 10c–10f), increased solar radiation (Drushka et al., 2014) or increased precipitation over evaporation (Zhang et al., 2015). For February 2016, in the different regions, the negative MLD anomalies correlated well with linear relationships for the positive total heat flux anomalies, and positive latent heat flux anomalies caused by weakened winds (Figures 13b–13d). While February 2016 had strongly negative precipitation minus evaporation anomalies, these conditions would act to destabilize the upper water column and deepen the MLD (Figure 13e). Hence the air-sea heat fluxes, and wind stress reduction were likely the dominant contribution to the MLD shoaling.

The positive air-sea heat fluxes can be trapped over the thinner MLD and enhance surface temperatures (e.g., Drushka et al., 2014; Zhang et al., 2015). This mechanism may be occurring in the build up to the maximum MHW intensities in early March 2016. The MLD anomalies reveal an asymmetry from the IAB to the Coral Sea, which may have consequences for warming patterns due to air-sea heat flux. During February
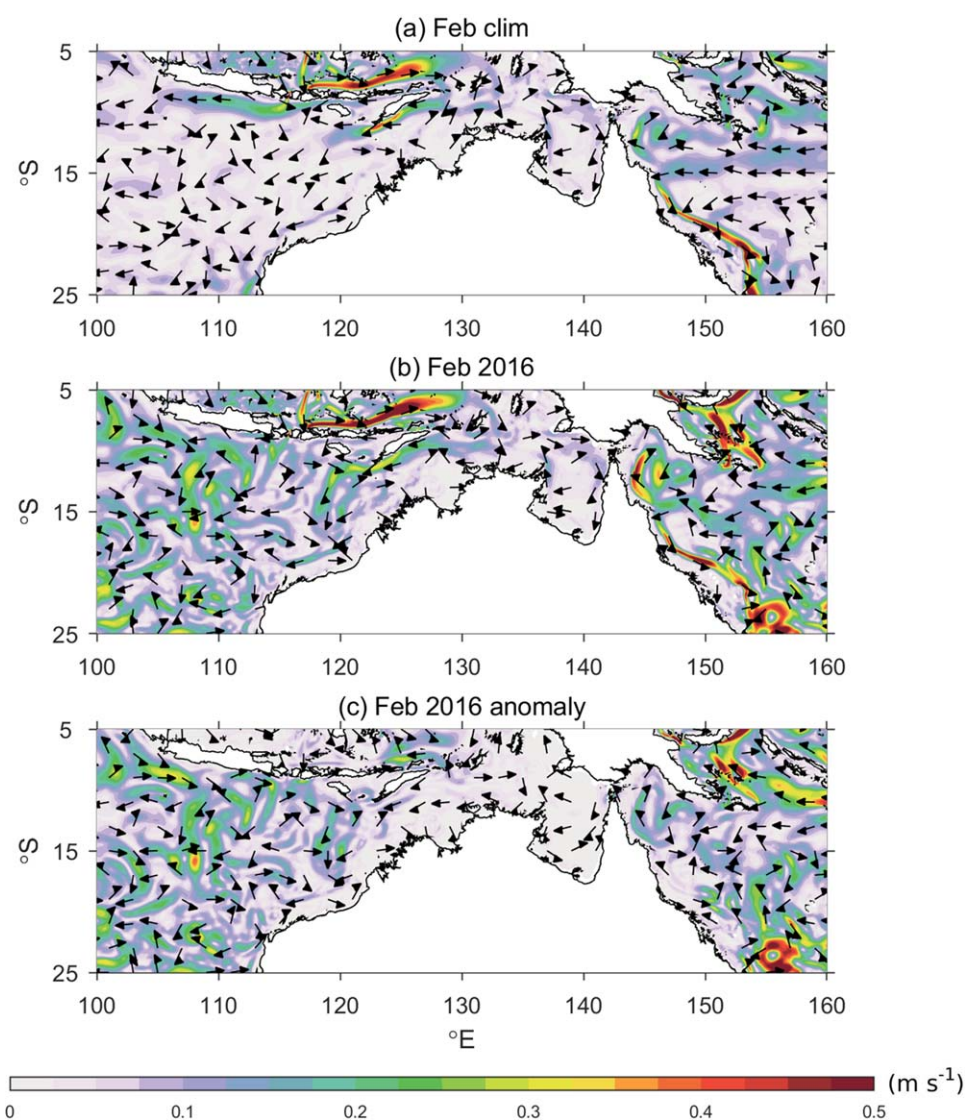
Figure 11. (a, b) Upper 100 m, depth averaged velocity from BRAN-2016, where speed is shaded and the arrows are unit vectors indicating direction; (c) depth averaged velocity anomaly compared with 1994–2015.

2016, the thinner MLD in the IAB (Figure 12e) combined with the stronger air-sea heat flux anomaly (Figure 9i), may explain why the IAB experienced more intense MHWs than in the Coral Sea (Figures 5b and 5j). Meanwhile, the reduced BLT may have played a role in the decay of the MHWs, as positive heat flux anomalies weakened in March 2016 (Figures 9j–9l), allowing for vertical entrainment of subsurface waters to have more of an impact on cooling upper ocean temperatures.

5. Comparison With Previous El Niño Periods

For waters around tropical Australia, the 2015–2016 MHW events that transpired were exceptional in their intensity and prolonged duration. In past El Niño events, warmer maximum SSTs occurred in tropical regions with a stronger signal in the SETIO than along the GBR (Eakin et al., 2009). Previous global coral bleaching events, which also manifest as tropical marine heatwaves, coincided with very strong El Niño periods, including 1982–1983 and 1997–1998, with reported moderate to severe bleaching around tropical Australia and only sparse reports in 1982–1983 (Oliver et al., 2009). However, the relationship between El Niño, based on the Niño3.4 SST, and bleaching events is not clear for some areas, such as the GBR having an ambiguous statistical relationship (Oliver et al., 2009). This may be due to regional-scale variability,
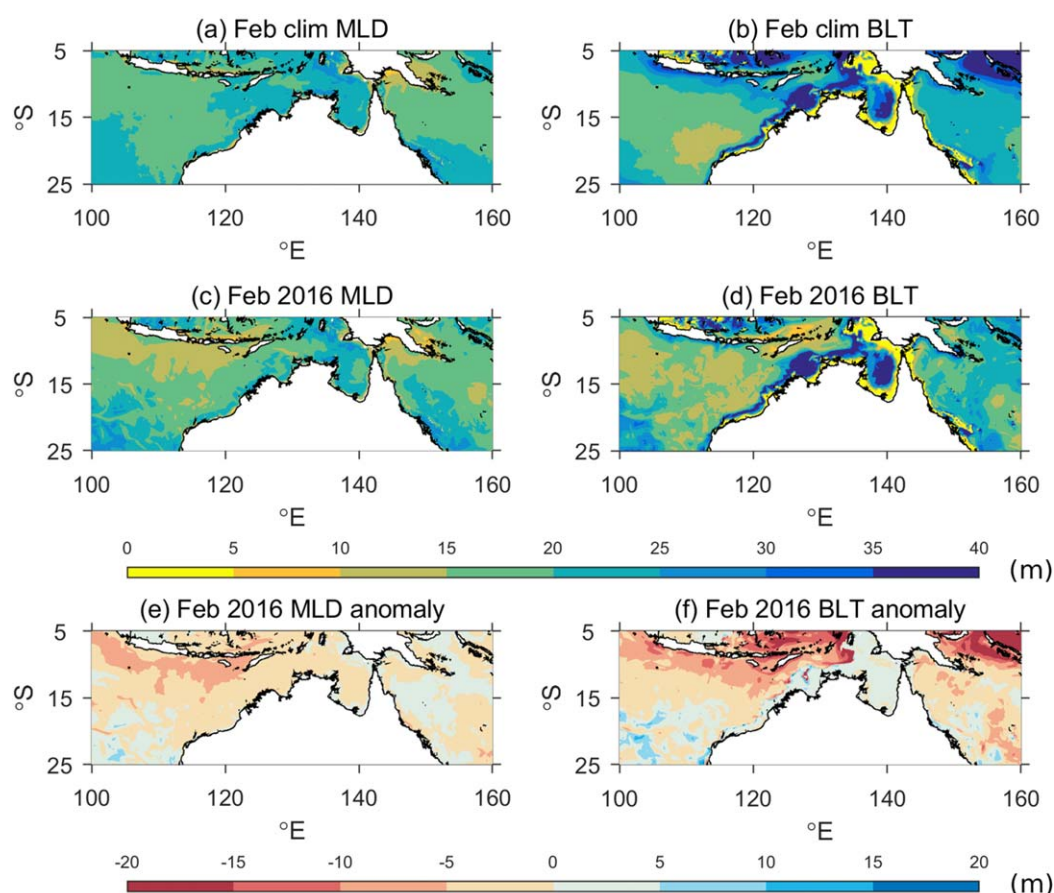
Figure 12. (a, c) Mixed layer depth (MLD) and anomaly compared with 1994–2015; (c, d) barrier layer thickness (BLT) and anomaly compared with 1994–2015. In plots a–d, values greater than 40 m are blue. In plots e and f, negative anomalies indicate shoaling and positive values indicate deepening, and values less than −20 m are red.

independent of the El Niño Southern Oscillation, owing to weather, ocean circulation, and timing of SST anomalies. Composite analyses for El Niño periods indicate there are significant warm SST anomalies in austral summer and autumn in the SETIO (Zhang et al., 2017), but for the GBR, significant warm SST anomalies occur only in autumn (Zhang et al., 2017), a late peak compared with the annual cycle (Lough, 1999).

For 1982–1983 and 1997–1998 El Niño periods, there are similarities and notable differences in MHW metrics for events occurring during the extended austral summer. These years were characterized by large Niño3.4 SST indices (Figure 1b) and weakened zonal winds in summer (Figure 1d). For both periods, the maximum SST showed the warmest waters occurring from the Kimberley shelf, Timor Sea, and into the GoC from December to February (Figures 14a–14d). The timing of the greatest MHW intensities tended to align with this time, amplifying the SST (Figures 14c, 14d, 14g, 14h). During 1982–1983, the most intense MHWs occurred off the North West Shelf and into the SETIO, whereas the Coral Sea was largely unaffected by MHWs (Figure 14e). During 1997–1998, the most intense MHWs occurred in widespread areas offshore of Australia in the IAB, GoC, Gulf of Papua, and the Southern GBR (Figure 14f). In both periods, total MHW durations persisted 1–3 months and the peak MHW intensities varied more regionally between December through April. In comparison, 2015–2016 showed a more extensive region around tropical Australia impacted by MHWs over a greater duration with a peak in MHW intensities during March (Figure 4). For 2015–2016, the MHWs were more intense in the Coral Sea and GBR, and almost all regions had the longest total duration compared with the past events (Figures 14i and 14j). There were a number of factors that contributed to this recent event compared to past events, including anomalies in the regional atmospheric conditions brought on by the El Niño, timing of extreme weather events, and the long-term warming trend.
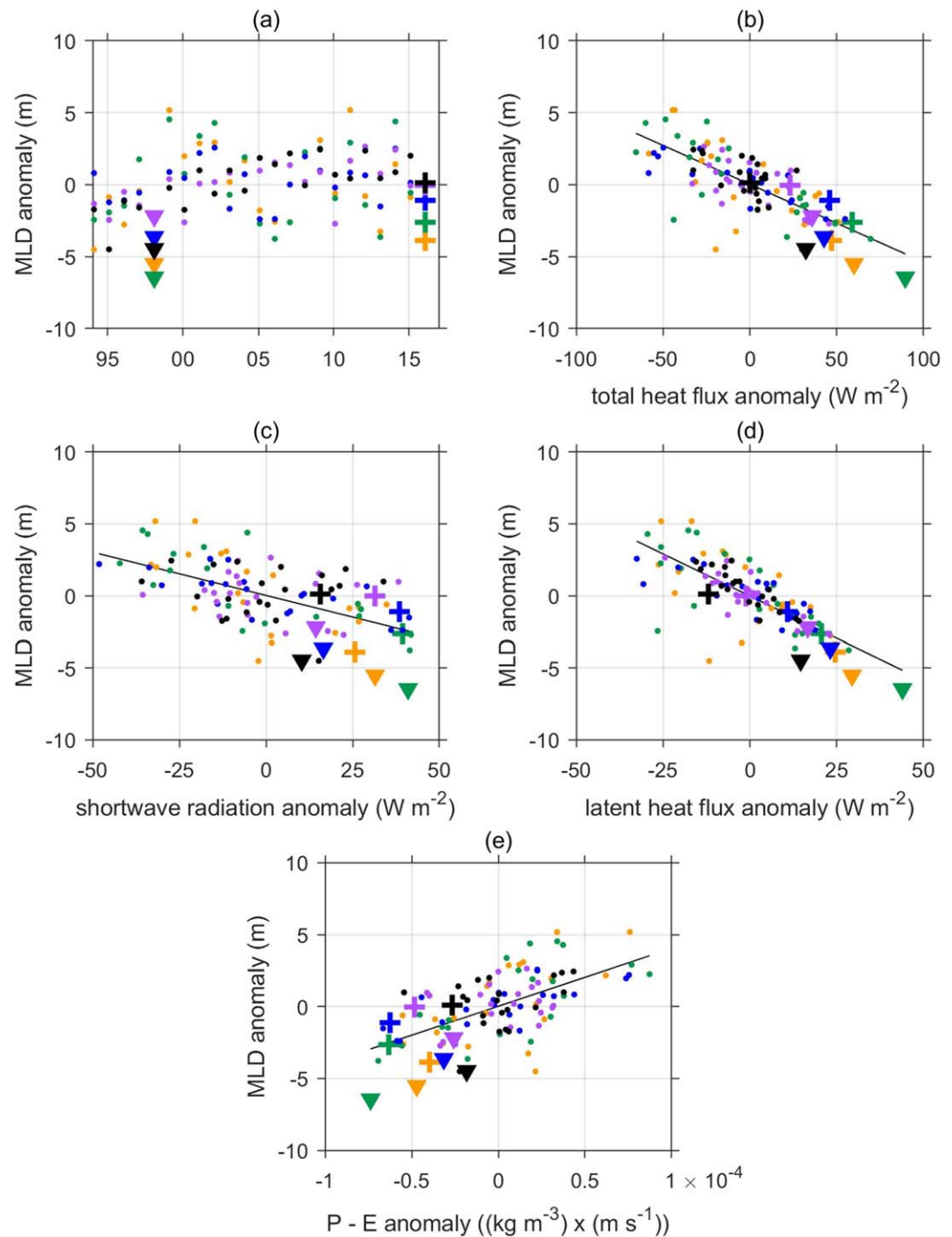
Figure 13. Comparison of the domain averaged mixed layer depth (MLD) and atmospheric forcing in February from the regions shown in Figure 2 with colors shown in Figure 6. (a) MLD anomalies from 1994 to 2016. MLD anomalies compared with (b) the total heat flux anomaly, (c) shortwave radiation anomaly, (d) latent heat flux anomaly, and (e) precipitation minus evaporation (P–E) anomaly. The symbols correspond to 1998 (▼), 2016 (+), and all other years (•). The best-fit linear curve (solid lines) are included in (b–e), and the R-square coefficients are (b) 0.57, (c) 0.35, (d) 0.58, and (e) 0.38.

Based on the data-assimilating model, the atmospheric and oceanic conditions contributing to the MHWs during 1997–1998 and 2015–2016 El Niños were exceptional. In both years, in which February conditions were compared from 1994 to 2016, there were notable negative MLD anomalies, increased air-sea heat flux into the ocean, and increased evaporation over precipitation (Figure 13). Hence the regional-scale forcing conditions for 2016 were consistent with the main features of the last major El Niño but with some
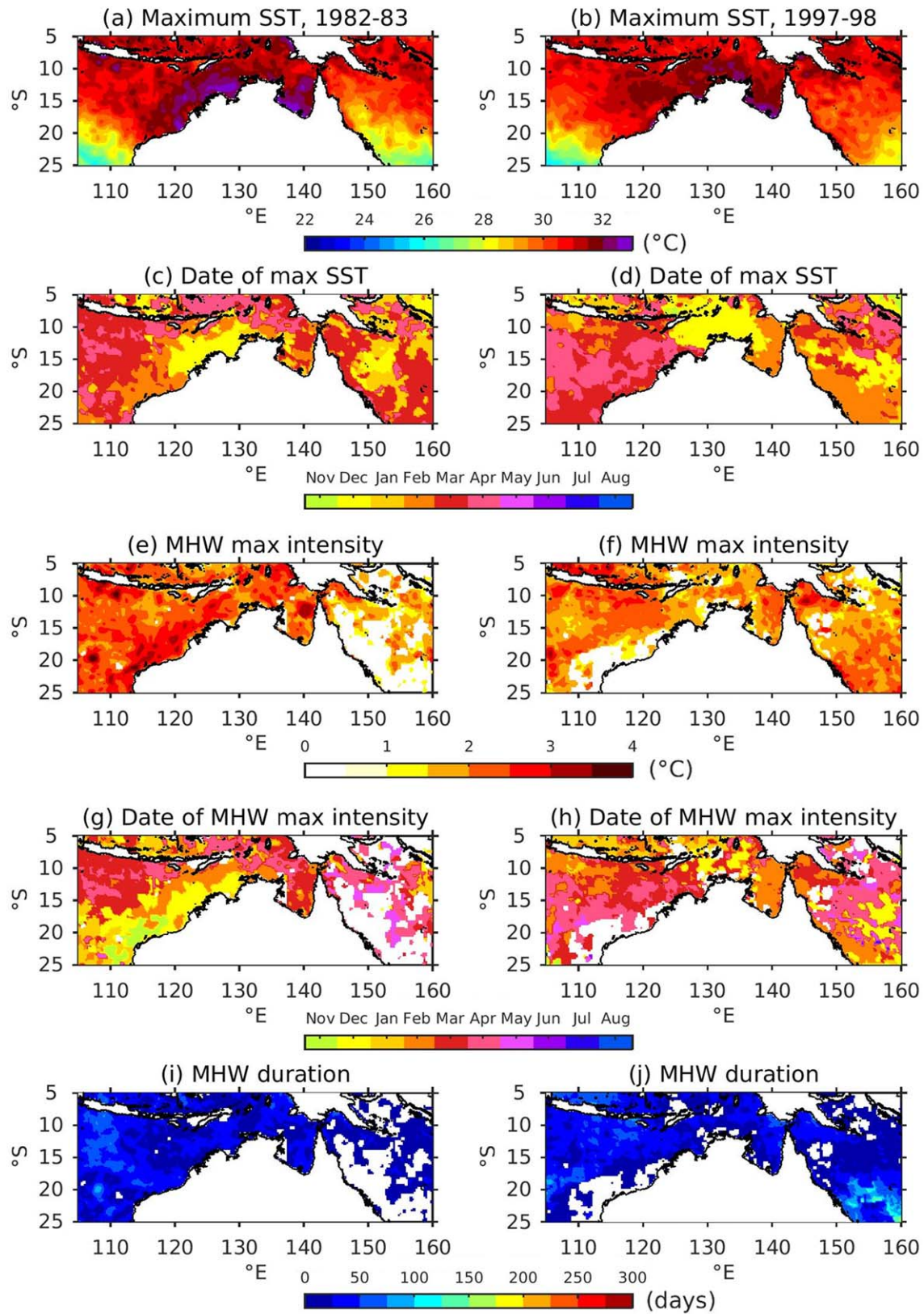
Figure 14. MHW metrics from NOAA OISST V2 from strong El Niño years 1982–1983 (left plots) and 1997–1998 (right plots). (a, b) Maximum SST detected during $T_{ext-summer}$ (1 November to 30 April); (c, d) Date of maximum SST shown in plots a and b; (e, f) the greatest maximum intensity (°C) from all MHWs during $T_{ext-summer}$; (g, h) Date of MHW maximum intensity shown in plots e and f; (i, j) the total duration of all MHWs which comenced during $T_{ext-summer}$.

differences. For 1998, the MLD anomalies were more strongly negative, there was more positive air-sea heat flux into the ocean, as well as a greater evaporation over precipitation anomaly (Figures 13a and 13b). Nevertheless, we found that the MHWs arising in 2015–2016 tended to be more intense and longer duration.

The timing of weather events and other oceanic phenomena may explain spatial variations in MHW intensity characteristics. In February 2016, tropical cyclone (TC) Stan cooled the North West Shelf (Bureau of Meteorology, 2016c; Hughes et al., 2017) and TC Winston cooled the Southern GBR (Bainbridge, 2017). A cool spot located off the North West Cape indicated a Ningaloo Niña, a cool event off the west coast of Australia, which commenced in December 2015 (Figure 3g). This cool anomaly could have occurred due to strengthened, upwelling favorable southerly wind anomalies (Kataoka et al., 2014), the divergence of the surface Ekman flow, or a negative air-sea heat flux anomaly (Figure 9c). Furthermore, for past El Niño periods, in January 1983, TC Des impacted the Central GBR, and in January 1998, long-lived TC Katrina persisted in the Coral Sea followed by TC Nathan 2 months later, TC Les traversed the Gulf of Carpentaria, and TC Tiffany passed along the North West Shelf (Bureau of Meteorology, http://www.bom.gov.au). From these severe weather events, the associated cloud cover and reduced radiative heating may have caused cooling (Leahy et al., 2013), in addition to turbulent entrainment of cooler, deeper waters (Glenn et al., 2016). These cyclones may have reduced the MHW intensities or suppressed MHW events altogether. Hence the timing of these extreme weather events impacted the regional characteristics of the MHWs that arose during the strong El Niños.

Finally, long-term warming over the past several decades contributed to the intensity and duration of the summer 2016 MHW. From calculating MHW properties from the entire domain averaged time series shown in Figure 1a, the most intense (+1.7°C) and longest (217 days) MHW on record occurred from 13 January to 16 August 2016 (supporting information Figure S10a). However, when the linear trend (calculated over 1982–2016) was removed and the MHW properties recalculated, the 2016 MHW was broken up into three shorter events (65, 11, and 72 days each) for a total of 148 MHW days and with a weaker maximum intensity of +1.4°C (supporting information Figure S10b). This finding is consistent with Oliver et al. (2017), which used global climate models and found that the intensity and duration of the 2016 MHW in tropical Australia was several times more likely in a world with anthropogenic forcing than in a natural-only world.

6. Discussion and Summary

Marine ecosystems, from the deep ocean to coastal regions, exist in balance within a thermal range, which may vary over decades and seasons but is also punctuated by extreme events such as MHWs. Off Western Australia and the North West Shelf, primary drivers of coral reef calcification rates, important for maintaining the reef systems, include the annual and winter minimum SST, with anomalously high rates in the south possibly due to the warm Leeuwin Current (Lough et al., 2016). At the same time, SST is the primary variable for predicting coral bleaching thresholds based on accumulated thermal stress, when water temperatures exceed typical environmental conditions (e.g., Berkelmans, 2002). In 2016, spatial patterns in recorded bleaching along the GBR followed spatial patterns of heat stress (Hughes et al., 2017). In addition, these severity patterns for the GBR and sites off North West Australia and Arnhem Land are consistent with the spatial patterns of maximum intensity and total duration recorded for MHWs during the extended austral summer (Figures 4e and 4f). Around tropical Australia, the sites with the lowest bleaching severity (Hughes et al., 2017) coincided generally with regions of lower MHW intensity or shorter duration or regions without any MHW recorded.

While MHWs can have a direct impact on species through thermal stress, especially in summer, the timing of warming can have other implications for marine ecosystems. For tropical Australia, some of the most intense and longest duration MHWs occurred during winter 2016. MHWs occurring post-summer coral bleaching can have implications for coral recovery and susceptibility to disease (e.g., Bruno et al., 2007; Ward et al., 2007) and so this cool-season warm period may have exacerbated the effects of the summer-time MHWs. Furthermore, near-surface warming increases the stratification, reducing vertical mixing with deeper oceanic waters, and potentially changing the depth of upwelling waters and nutrient sources (García-Reyes et al., 2015). For 2016, in the Central GBR, typical upwelling events appeared to have been suppressed during the peak of the MHW, compared with past years during the same month (Benthuysen et al., 2016). The Slocum gliders revealed that the warm waters were found from midshelf to the shelf break

over hundreds of kilometers and even in the reef passages known for intrusive upwelling (Figures 8c and 8d). Off Java in 2016, some of the most intense MHWs occurred in regions affected for the longest total duration (Figures 4e and 4f). Upwelling typically occurs here from June to October due to southeasterly monsoon winds (Susanto et al., 2001). During El Niño periods, the thermocline depth becomes shallower off Java and Sumatra, with cooler water flowing into the Indian Ocean through the Indonesian Seas (Susanto et al., 2001). However, for 2016, the IAB waters experienced the longest duration and most intense MHW during winter (Figure 5b) with some of the greatest SST anomalies off Java (Figure 4, June–September 2016). Winter-spring 2016 had one of the strongest negative Indian Ocean Dipole events, corresponding to warmer than normal SST in the IAB and off northwest Australia (Oliver et al., 2017). Furthermore, 2016 had a rapid transition from El Niño conditions in autumn to a weak La Niña by late winter (Figure 1b) which, based on composite analyses (e.g., Zhang et al., 2017), would support the persistence of warm anomalies in the MHW region beyond autumn. The interactions between these climate modes of variability and their influences on winds, air-sea heat fluxes, and the upper ocean mixed layer structure merit future investigation into their roles in spatial patterns and timing of MHWs and subsequent consequences on regional marine ecosystems.

The 2015–2016 MHWs across tropical Australia highlight the rapid onset of SST anomalies and the late peak in SST in some regions. Progress in understanding how climate modes of variability impact the emergence of regional MHWs will improve preparations for monitoring coral bleaching events and other marine ecosystem disturbances. On a regional scale, long-term monitoring provides the baseline understanding of in situ temperature and links with meteorological variability and the ecosystem state. For waters affected by MHWs spanning ocean basins, such observations are required as part of a national framework. In remote areas, engagement with the local communities is essential for improving the monitoring of marine environments with sparse and discrete observations. Importantly, public awareness of the environment and detected changes and the efficient communication of those findings provide key information on areas warranting scientific investigation. As a MHW event unfolds, a rapid response by the scientific community requires access to near-real time observations, such as coral reef observing stations and weather station data (http://weather.aims.gov.au/#/overview; Bainbridge, 2017) and remotely sensed SST as utilized by products including the National Oceanic and Atmospheric Administration (NOAA) Coral Reef Watch (https://coralreefwatch.noaa.gov.au). In situ temperatures recorded by a ship's underway system and comparison with available high resolution climatologies and percentiles provide another source for improving near-real time MHW detection. Given the prolonged nature of the 2015–2016 warming event beyond the summer peak, an integrated approach to monitoring affected areas from the oceanographic to ecosystem scale will provide insight into how marine ecosystems are altered, persevere, and recover from such massive events.

In summary, this study presents comprehensive documentation of the extreme ocean warming events around tropical Australia during 2015–2016. From remotely sensed SST, marine heatwaves emerged in all surrounding regions by January 2016, peaked in March 2016, and persisted throughout the following winter season. This broad scale perspective was complemented by coastal in situ temperature loggers that also showed consistent timing in the marine heatwaves development and decay. The loggers provided further spatial information on MHW characteristics from east to west, near-shore to shelf, and with depth. High temporal and spatial resolution are provided by in situ temperature measurements from the underway system onboard the R/V Solander over the North West Shelf, the Slocum gliders in the GBR, and the Argo float in the Coral Sea. These observations combined highlight the extraordinary extent of warming throughout these regions. The warming event occurred during a strong El Niño period, with weakened monsoon activity modulated by the MJO, and superimposed on a long-term warming trend. In January and February 2016, enhanced shortwave radiation and reduced evaporative cooling contributed to net air-sea heat flux anomalies into the ocean. Based on a data-assimilating ocean model, regions from the IAB to the Coral Sea tended to have thinner surface mixed layer depths and barrier layer thicknesses than usual. The upper ocean circulation indicated regional areas with intensified or weakened currents along boundaries and in the open ocean but these changes have yet to be directly attributed to the 2015–2016 El Niño event. Further investigations with a freely evolving ocean model can be used to construct regional heat budgets and diagnose the particular roles of air-sea heat fluxes, winds, circulation patterns, and vertical mixing during the generation and decay of the marine heatwaves contributing to this extreme warming event.

References

AIMS (2017a). *Sea water temperature logger data at Lizard Island, Great Barrier Reef from 27 Oct 1995 to 06 Dec 2014*. Retrieved from http://data.aims.gov.au/metadataviewer/faces/view.xhtml?uuid=b8fc8578-fef9-43fa-9483-222ade016c2b, accessed 23 Feb 2017

AIMS (2017b). *Sea water temperature logger data at Thursday Island, Torres Strait from 12 May 1998 to 12 Sep 2013*. Retrieved from http://data.aims.gov.au/metadataviewer/faces/view.xhtml?uuid=8cd23149-24b4-4737-9c22-6e15cfe8602a, accessed 22 Feb 2017

AIMS (2017c). *Thursday Island weather station 2 water temperature: From 01 Feb 2012 to 07 Jan 2017 (NERP TE Project 2.3)*. Retrieved from http://data.aims.gov.au/metadataviewer/faces/view.xhtml?uuid=eb17fa84-6ead-4323-9715-a26c20c78e82, accessed 22 Feb 2017

AIMS (2017d). *Thursday Island weather station water temperature: From 08 Feb 2012 to 19 Jul 2014 (NERP TE Project 2.3)*. Retrieved from http://data.aims.gov.au/metadataviewer/faces/view.xhtml?uuid=44ffebf4-e636-4f8c-9355-2c01178bede4, accessed 22 Feb 2017

AIMS (2016). *Western Australian reefs feel the heat from global bleaching event*. Queensland, Australia: Australian Institute of Marine Science. Retrieved from http://www.aims.gov.au/docs/media/featured-content.html/

Allan, R. J., & Pariwono, J. I. (1990). Ocean-atmosphere interactions in low-latitude Australasia. *International Journal of Climatology*, *10*(2), 145–178. https://doi.org/10.1002/joc.3370100204

Bainbridge, S. J. (2017). Temperature and light patterns at four reefs along the Great Barrier Reef during the 2015–2016 austral summer: Understanding patterns of observed coral bleaching. *Journal of Operational Oceanography*, *10*(1), 16–29. https://doi.org/10.1080/1755876X.2017.1290863

Benthuysen, J. A., Tonin, H., Brinkman, R., Herzfeld, M., & Steinberg, C. (2016). Intrusive upwelling in the Central Great Barrier Reef. *Journal of Geophysical Research: Oceans*, *121*, 8395–8416. https://doi.org/10.1002/2016JC012294

Berkelmans, R. (2002). Time-integrated thermal bleaching thresholds of reefs and their variation on the Great Barrier Reef. *Marine Ecology Progress Series*, *229*, 73–82.

Bruno, J. F., Selig, E. R., Casey, K. S., Page, C. A., Willis, B. L., Drew Harvell, C., et al. (2007). Thermal stress and coral cover as drivers of coral disease outbreaks. *PLoS Biology*, *5*(6), e124. https://doi.org/10.1371/journal.pbio.0050124

Bureau of Meteorology (2016a). *Australian baseline sea level monitoring array monthly data report–March 2016*. Melbourne, Australia: Bureau of Meteorology.

Bureau of Meteorology (2016b). *Monthly weather review Australia December 2015*. Melbourne, Australia: Bureau of Meteorology.

Bureau of Meteorology (2016c). *Monthly weather review Australia January 2016*. Melbourne, Australia: Bureau of Meteorology.

Bureau of Meteorology (2016d). *Monthly weather review Australia February 2016*. Melbourne, Australia: Bureau of Meteorology.

Bureau of Meteorology (2016e). *Monthly weather review Australia March 2016*. Melbourne, Australia: Bureau of Meteorology.

Dee, D. P., Uppala, S. M., Simmons, A. J., Berrisford, P., Poli, P., Kobayashi, S., et al. (2011). The Era-Interim reanalysis: Configuration and performance of the data assimilation system. *Quarterly Journal of the Royal Meteorological Society*, *137*, 553–597. https://doi.org/10.1002/qj.828

Drushka, K., Sprintall, J., & Gille, S. T. (2014). Subseasonal variations in salinity and barrier-layer thickness in the eastern equatorial Indian Ocean. *Journal of Geophysical Research: Oceans*, *119*, 805–823. https://doi.org/10.1002/2013JC009422

Du, Y., Qu, T., & Meyers, G. (2008). Interannual variability of sea surface temperature off Java and Sumatra in a global GCM. *Journal of Climate*, *21*(11), 2451–2465. https://doi.org/10.1175/2007JCLI1753.1

Duke, N. C., Kovacs, J. M., Griffiths, A. D., Preece, L., Hill, D. J. E., van Oosterzee, P., et al. (2017). Large-scale dieback of mangroves in Australia's Gulf of Carpentaria: A severe ecosystem response, coincidental with an unusually extreme weather event. *Marine and Freshwater Research*, *68*(10), 1816–1829. https://doi.org/10.1071/MF16322

Eakin, C. M., Lough, J. M., & Heron, S. F. (2009). Climate variability and change: Monitoring data and evidence for increased coral bleaching stress. In M. Van Oppen & J. M. Lough (Eds.), *Coral bleaching: Patterns, processes, causes and consequences, Ecological Studies 205* (178 pp.). Berlin, Germany: Springer.

Evans, J. L., & Allen, R. J. (1992). El Nino/Southern oscillation modification structure of the monsoon and tropical activity in the Australasian region. *International Journal of Climatology*, *12*, 611–623. https://doi.org/10.1002/joc.3370120607

García-Reyes, M., Sydeman, W. J., Schoeman, D. S., Rykaczewski, R. R., Black, B. A., Smit, A. J., et al. (2015). Under Pressure: Climate Change, Upwelling, and Eastern Boundary Upwelling Ecosystems. *Frontiers in Marine Science*, *2*(109), 1–10. https://doi.org/10.3389/fmars.2015.00109

Glenn, S. M., Miles, T. N., Seroka, G. N., Xu, Y., Forney, R. K., Yu, F., et al. (2016). Stratified coastal ocean interactions with tropical cyclones. *Nature Communications*, *7*, https://doi.org/10.1038/ncomms10887

GBRMPA (2016). *Interim report: 2016 coral bleaching event on the Great Barrier Reef*. Townsville, Australia: Great Barrier Reef Marine Park Authority. Retrieved from http://hdl.handle.net/11017/3044

Harris, T., Hope, P., Oliver, E., Smalley, R., Arblaster, J., Holbrook, N., et al. (2017). *Climate drivers of the 2015 Gulf of Carpentaria mangrove dieback* (Earth Systems and Climate Change Hub Tech. Rep. No. 1). Australia: NESP Earth Systems and Climate Change Hub.

Hendon, H. H., & Liebmann, B. (1990). The intraseasonal (30–50 day) oscillation of the Australian summer monsoon. *Journal of the Atmospheric Sciences*, *47*(24), 2909–2923. https://doi.org/10.1175/1520-0469(1990)047 < 2909:TIDOOT>2.0.CO;2

Heron, S. F., Maynard, J. A., van Hooidonk, R., & Eakin, C. M. (2016). Warming trends and bleaching stress of the world's Coral Reefs 1985–2012. *Scientific Reports*, *6*, 38402. https://doi.org/10.1038/srep38402

Hobday, A. J., Alexander, L. V., Perkins, S. E., Smale, D. A., Straub, S. C., Oliver, E. C., et al. (2016). A hierarchical approach to defining marine heatwaves. *Progress in Oceanography*, *141*, 227–238. https://doi.org/10.1016/j.pocean.2015.12.014

Hughes, T. P., Kerry, J. T., Álvarez-Noriega, M., Álvarez-Romero, J. G., Anderson, K. D., Baird, A. H., et al. (2017). Global warming and recurrent mass bleaching of corals. *Nature*, *543*(7645), 373–377. https://doi.org/10.1038/nature21707

Hung, C.-W., & Yanai, M. (2004). Factors contributing to the onset of the Australian summer monsoon. *Quarterly Journal of the Royal Meteorological Society*, *130*(597), 739–758. https://doi.org/10.1256/qj.02.191

IMOS (2017a). *IMOS FAIMMS sensor network data–Lizard Island relay pole 2 water temperature–From 14 Aug 2010 to 15 Dec 2016*. Retrieved from http://data.aims.gov.au/metadataviewer/faces/view.xhtml?uuid=8151be9e-ff95-4ca6-aeae-7630e69e643c, accessed 23 Feb 2017

IMOS (2017b). *IMOS FAIMMS sensor network data–Lizard Island sensor float 2 water temperature–From 13 Aug 2010 to 14 Nov 2016*. Retrieved from http://data.aims.gov.au/metadataviewer/faces/view.xhtml?uuid=8bcedc63-0bf1-47a7-80fd-5f47903b25bd, accessed 23 Feb 2017

Joseph, P. V., Liebmann, B., & Hendon, H. H. (1991). Interannual Variability of the Australian Summer Monsoon Onset: Possible Influence of Indian Summer Monsoon and El Niño. *Journal of Climate*, *4*(5), 529–538. https://doi.org/10.1175/1520-0442(1991)004 < 0529:IVOTAS>2.0.CO;2

Kajikawa, Y., Wang, B., & Yang, J. (2010). A multi-time scale Australian monsoon index. *International Journal of Climatology*, *30*(8), 1114–1120. https://doi.org/10.1002/joc.1955

Kanamitsu, M., Ebisuzaki, W., Woollen, J., Yang, S.-K., Hnilo, J. J., Fiorino, M., et al. (2002). NCEP-DOE AMIP-II reanalysis (R-2). *Bulletin of the American Meteorological Society*, 83, 1631–1643. https://doi.org/10.1175/BAMS-83-11-1631

Kataoka, T., Tozuka, T., Behera, S., & Yamagata, T. (2014). On the Ningaloo Niño/Niña. *Climate Dynamics*, *43*(5–6), 1463–1482. https://doi.org/10.1007/s00382-013-1961-z

King, A. D., Karoly, D. J., & Henley, B. J. (2017). Australian climate extremes at 1.5°C and 2°C of global warming. *Nature Climate Change*, 7, 412–416. https://doi.org/10.1038/nclimate3296

Klein, S. A., Soden, B. J., & Lau, N.-C. (1999). Remote sea surface temperature variations during ENSO: Evidence for a tropical atmospheric bridge. *Journal of Climate*, *12*(4), 917–932. https://doi.org/10.1175/1520-0442(1999)012 < 0917:RSSTVD>2.0.CO;2

Leahy, S. M., Kingsford, M. J., & Steinberg, C. R. (2013). Do clouds save the Great Barrier Reef? Satellite imagery elucidates the cloud-SST relationship at the local scale. *PLOS One*, *8*(7), e70400. https://doi.org/10.1371/journal.pone.0070400

Liu, G., Skirving, W., & Strong, A. E. (2003). Remote sensing of sea surface temperatures during 2002 Barrier Reef coral bleaching. *EOS, Transactions, American Geophysical Union*, *84*(15), 137–144. https://doi.org/10.1029/2003EO150001

Liu, G., Strong, A. E., Skirving, W. J., & Arzayus, L. F. (2006). *Overview of NOAA Coral Reef watch program's near-real-time satellite global coral bleaching monitoring activities*. Paper presented at proceedings of the 10th International Coral Reef Symposium (Vol. 1, pp. 1783–1793), Okinawa, Japan.

Lough, J. M. (1994). Climate variation and El Niño-Southern oscillation events on the Great Barrier Reef: 1958 to 1987. *Coral Reefs*, 13, 181–195. https://doi.org/10.1007/BF00301197

Lough, J. M. (1999). *Sea surface temperatures on the Great Barrier Reef: A contribution to the study of coral bleaching* (Res. Publ. 57). Townsville, QLD: Great Barrier Reef Marine Park Authority. http://hdl.handle.net/11017/331

Lough, J. M. (2007). Chapter 2: Climate and climate change on the Great Barrier Reef. In J. E. Johnson & P. A. Marshall (Eds.), *Climate change and the Great Barrier Reef*. Australia: Great Barrier Reef Marine Park Authority and Australian Greenhouse Office.

Lough, J. M., Cantin, N. E., Benthuysen, J. A., & Cooper, T. F. (2016). Environmental drivers of growth in massive *Porites* corals over 16 degrees of latitude along Australia's northwest shelf. *Limnology and Oceanography*, *61*(2), 684–700. https://doi.org/10.1002/lno.10244

Madden, R. A., & Julian, P. R. (1971). Detection of a 40–50 day oscillation in the zonal wind in the tropical Pacific. *Journal of the Atmospheric Sciences*, *28*(5), 702–708. https://doi.org/10.1175/1520-0469(1971)028 < 0702:DOADOI>2.0.CO;2

Madden, R. A., & Julian, P. R. (1972). Description of global-scale circulation cells in the tropics with a 40–50 day period. *Journal of the Atmospheric Sciences*, *29*(6), 1109–1123. https://doi.org/10.1175/1520-0469(1972)029 < 1109:DOGSCC>2.0.CO;2

Mann, M. E., Rahmstorf, S., Steinman, B. A., Tingley, M., & Miller, S. K. (2016). The likelihood of recent record warmth. *Scientific Reports*, 6, 19831. https://doi.org/10.1038/srep19831

Meehl, G. A., & Arblaster, J. M. (1998). The Asian-Australian monsoon and El Niño-Southern oscillation in the NCAR climate system model. *Journal of Climate*, *11*(6), 1356–1385. https://doi.org/10.1175/1520-0442(1998)011<1356:TAAMAE>2.0.CO;2

Melet, A., Gourdeau, L., & Verron, J. (2010). Variability in Solomon Sea circulation derived from altimeter sea level data. *Ocean Dynamics*, *60*(4), 883–900. https://doi.org/10.1007/s10236-010-0302-6

Nicholls, N. (1979). A simple air-sea interaction model. *Quarterly Journal of the Royal Meteorological Society*, *105*(443), 93–105. https://doi.org/10.1002/qj.49710544307

NOAA (2017). *State of the climate: Global analysis for annual 2016*. Retrieved on February 22, from http://www.ncdc.noaa.gov/sotc/global/201613

NTSC (2016). *September mud crabs in focus*. Darwin, Australia: Newsletter of the Northern Territory Seafood Council. Retrieved from https://www.ntsc.com.au/documents/item/26

Oke, P., Sakov, P., Cahill, M. L., Dunn, J. R., Fiedler, R., Griffin, D. A., et al. (2013). Towards a dynamically balanced eddy-resolving reanalysis: BRAN3. *Ocean Modelling*, *67*, 52–70. https://doi.org/10.1016/j.ocemod.2013.03.008

Oliver, J. K., Berkelmans, R., & Eakin, C. M. (2009). Coral bleaching in space and time. In M. Van Oppen & J. M. Lough (Eds.), *Coral bleaching: Patterns, processes, causes and consequences*, Ecological Studies 205 (178. pp.). Berlin, Germany: Springer.

Oliver, E. C. J., Perkins-Kirkpatrick, S. E., Holbrook, N. J., & Bindoff, N. L. (2017). Anthropogenic and natural influences on record 2016 marine heatwaves (in "Explaining extreme events of 2016 from a climate perspective"). *Bulletin of the American Meteorological Society*, *98*(12), S44–S48. https://doi.org/10.1175/BAMS-D-17-0093.1

Redondo-Rodriguez, A., Weeks, S. J., Berkelmans, R., Hoegh-Guldberg, O., & Lough, J. M. (2012). Climate variability of the Great Barrier Reef in relation to the tropical Pacific and El Niño-Southern oscillation. *Marine and Freshwater Research*, *63*(1), 34–47. https://doi.org/10.1071/MF11151

Reynolds, R. W., Smith, T. M., Liu, C., Chelton, D. B., Casey, K. S., & Schlax, M. G. (2007). Daily high-resolution-blended analyses for sea surface temperature. *Journal of Climate*, *20*(22), 5473–5496. https://doi.org/10.1175/2007JCLI1824.1

Reynolds, R. W., Rayner, N. A., Smith, T. M., Stokes, D. C., & Wang, W. (2002). An improved in situ and satellite SST analysis for climate. *Journal of Climate*, *15*(13), 1609–1625. https://doi.org/10.1175/1520-0442(2002)015 < 1609:AIISAS>2.0.CO;2

Ridgway, K. R., Dunn, J. R., & Wilkin, J. L. (2002). Ocean interpolation by four-dimensional least squares – Application to the waters around Australia. *Journal of Atmospheric and Oceanic Technology*, *19*(9), 1357–1375. https://doi.org/10.1175/1520-0426(2002)019 < 1357:OIBFDW>2.0.CO;2

Saji, N. H., Goswami, B. N., Vinayachandran, P. N., & Yamagata, T. (1999). A dipole mode in the tropical Indian Ocean. *Nature*, *401*(6751), 360–363. https://doi.org/10.1038/43854

Susanto, R. D., Gordon, A. L., & Zheng, Q. (2001). Upwelling along the coasts of Java and Sumatra and its relation to ENSO. *Geophysical Research Letters*, *28*(8), 1599–1602. https://doi.org/10.1029/2000GL011844

Ward, J. R., Kim, K., & Harvell, C. D. (2007). Temperature affects coral disease resistance and pathogen growth. *Marine Ecology Progress Series*, *329*, 115–121.

Wild, K. (2016). Indigenous rangers on the frontline of coral bleaching in remote Australia. *Australian Broadcasting Corporation*. Retrieved from http://www.abc.net.au/news/2016-07-11/indigenous-rangers-on-the-frontline-of-coral-bleaching/7557646

Xie, S. P., & Philander, S. G. H. (1994). A coupled ocean-atmosphere model of relevance to the ITCZ in the eastern Pacific. *Tellus A*, *46*(4), 340–350. https://doi.org/10.1034/j.1600-0870.1994.t01-1-00001.x

Xie, S. P., Hu, K., Hafner, J., Tokinaga, H., Du, Y., Huang, G., et al. (2009). Indian Ocean capacitor effect on Indo-western Pacific climate during the summer following El Niño. *Journal of Climate*, *22*(3), 730–747. https://doi.org/10.1175/2008JCLI2544.1

Xie, S. P., Kosaka, Y., Du, Y., Hu, K., Chowdary, J. S., & Huang, G. (2016). Indo-western Pacific Ocean capacitor and coherent climate anomalies in post-ENSO summer: A review. *Advances in Atmospheric Sciences*, *33*(4), 411–432. https://doi.org/10.1007/s00376-015-5192-6

Zhang, R.-H., Gao, C., Kang, X., Zhi, H., Wang, Z., & Feng, L. (2015). ENSO modulations due to interannual variability of freshwater forcing and ocean biology-induced heating in the tropical Pacific. *Scientific Reports*, *5*, 18506. https://doi.org/10.1038/srep18506

Zhang, N., Feng, M., Du, Y., Lan, J., & Wijffels, S. E. (2016). Seasonal and interannual variations of mixed layer salinity in the southeast tropical Indian Ocean. *Journal of Geophysical Research: Oceans*, *121*, 4716–4731. https://doi.org/10.1002/2016JC011854

Zhang, N., Feng, M., Hendon, H. H., Hobday, A. J., & Zinke, J. (2017). Opposite polarities of ENSO drive distinct patterns of coral bleaching potentials in the southeast Indian Ocean. *Scientific Reports*, *7*(1), 2443. https://doi.org/10.1038/s41598-017-02688-y